Temporal Regularization of the P_N Equations*

Cory D. Hauck
Computational Physics and Methods (CCS-2) &
Center for Nonlinear Studies (CNLS)
Los Alamos National Laboratory
cdhauck@lanl.gov

Robert B. Lowrie
Computational Physics and Methods (CCS-2)
Los Alamos National Laboratory
lowrie@lanl.gov

August 7, 2008

Abstract

In this paper, we introduce a regularization of the P_N equations for one-dimensional, slab geometries. These equations are used to describe particle transport through a material medium. Our regularization is based on a temporal splitting of fast and slow dynamics in the P_N system. It uses ideas first introduced in [14] for 2×2 systems to address systems of arbitrary size and with spatially varying media. The regularization captures the proper diffusion limit in diffusive regimes, but behaves like the original P_N system in streaming regimes. It also allows for larger times steps in diffusive regimes, when the original P_N system is stiff. In particular, for simulations in which the computational mesh does not resolve the particle mean-free-path, the regularization admits a simple scheme with no stability restrictions on the time step.

Keywords: *diffusive relaxation, stiff relaxation, transport theory, P_N equations, temporal regularization, operator splitting*
AMS classification: 65M99, 65Z05, 35F10, 82D75, 78M05

1 Introduction

In a kinetic description, the transfer of neutral particles through a material medium is governed by a transport equation, generally of the form

$$\partial_t F + v \cdot \nabla_x F = \mathcal{C}(F)\,. \tag{1}$$

*Los Alamos Report LA-UR-07-7995

Here $x \in \Omega \subset \mathbb{R}^3$ is a spatial coordinate, $v \in \mathbb{R}^3$ is a velocity coordinate, $t \geq 0$ is time, and the function $F = F(v, x, t)$ is the non-negative distribution of particles in position-momentum phase space. The left-hand side of (1) describes the evolution of F along inertial trajectories, while the collision operator $\mathcal{C}$ on the right-hand side describes particle interactions with the medium via scattering and absorption/emission processes.

One approach to solving (1) is with moment methods. In the moment approach, one tracks the evolution of a finite number of velocity moments of F. These moments, which are functions of space and time only, can then be used to reconstruct an approximation of F. Their evolution is approximated by a system of partial differential equations that are derived directly from (1). The exact form of these equations and the reconstruction of F is known as the *closure problem*. For most closures, the moment equations form a hyperbolic system.

When the material medium is fixed in space, there is typically a diffusive limit for (1) in which F is approximated by a non-negative scalar function of space and time that satisfies a diffusion equation. This approximation is valid when collision processes dominate, i.e., when the mean free path between collisions is small compared to macroscopic variations in the system. Because collisions drive particles into equilibrium with the fixed medium, long time scales are required in order to observe non-trivial dynamics. A basic requirement of any closure is that the resulting moment system has the same diffusion limit as the transport equation (1).

For numerical simulations, the hyperbolic nature of most moment systems and the parabolic nature of the diffusion approximation are not always compatible. As a consequence, the simulation of multi-scale problems with multiple temporal and spatial scales can be a challenge. In practice, there is a need for hyperbolic solvers that can handle shocks and discontinuities associated with streaming regimes (when the collisions are less frequent), but also behave like standard diffusion solvers in diffusive regimes. In particular, a hyperbolic solver should be consistent with the diffusion equation in the diffusion limit. This is the so-called *asymptotic preserving property* [14]. Unfortunately, hyperbolic solvers use numerical dissipation to maintain stability around discontinuities, and in most cases, this dissipation increases as the system approaches the diffusive limit. At some point, the numerical dissipation dominates the actual physical diffusion in the system. Consequently, one may generate results which appear correct (because they are smooth), but are far from accurate.

Another drawback of conventional hyperbolic solvers is a restrictive time step. In diffusive regimes, the relevant time scales are related to the macroscopic features of the system. However, hyperbolic solvers typically take time steps on the order of the (much smaller) particle mean flight time in order to maintain stability. As a result, the simulation of diffusive systems with hyperbolic solvers may be inefficient.

Extensive studies have been dedicated to the development of hyperbolic solvers which correctly capture the diffusion limit. We refer the reader to Section 3 for a brief overview of previous work, most of which has been limited to 2×2 systems in one dimension. The prototype model for such systems is the *hyperbolic heat equation* [15].

Our current interest is in simulating moment systems of arbitrary size—a task we found to be substantially more difficult than the 2×2 case. In the present paper, we focus our attention on the so-called P_N *equations* [21, 31], for which the reconstruction of F is a finite linear combination of polynomials in the velocity variable with coefficients that depend on

space and time. Here the letter 'P' is the conventional notation for these polynomials and the integer N refers to the order of the expansion. When $N = 1$, the P_N equations are equivalent to the hyperbolic heat equation.

We restrict the scope of our study to systems for which: (i) particles travel with a single speed (but different directions); (ii) $\mathcal{C}$ is a simple scattering operator; and (iii) the material medium has a slab geometry. This last assumption allows us to express the P_N system using only one spatial dimension. Future efforts will focus on extensions to more general nonlinear systems with more complicated physics and geometries.

The method presented here uses ideas from [14] to construct a temporal regularization of the original P_N system that is more amenable to numerical simulation. Our regularized system has two major benefits:

1. The diffusion limit is built directly into the equations. Thus numerical dissipation is not an issue. Moreover, diffusive terms can be discretized directly with simple, standard techniques.

2. The regularized system is less stiff. At worst, an explicit diffusion time step is required for stability. However, in cases where the numerical mesh spacing does not resolve the mean free path (so-called *under-resolved* cases), an implicit treatment of diffusion terms removes any stability-based restriction on the time step.

The organization of the paper is as follows. In Section 2, we derive the P_N equations under the simplified setting alluded to above. In Section 3, we discuss stiffness and excessive numerical dissipation in the context of the 2×2 P_1 system. We then present the method in [14] that was developed to address these challenges. In Section 4, we show how to extend this method from the P_1 system to the P_3 system when the scattering cross-section of the material medium is constant. In Section 5, we consider general P_N system with spatially varying cross-sections. In Section 6 we make conclusions and discuss future work.

2 The P_N Equations in One Dimension

We assume a distribution of particles of a single speed which scatter off a background with slab geometry, independently of their direction of travel. With a diffusive scaling, the transport equation takes the form

$$\partial_t F + \frac{1}{\varepsilon}\mu\partial_x F = -\frac{\sigma}{\varepsilon^2}\left(F - \frac{1}{2}\langle F\rangle\right). \tag{2}$$

In this simplified, one-dimensional setting, $x \in [x_0, x_1]$ is now the scalar coordinate along the axis perpendicular to a material slab, $\mu \in [-1, 1]$ is the cosine of the angle between the x-axis and the direction of particle travel, $t \geq 0$ is time, and for any measurable function $g = g(\mu)$,

$$\langle g\rangle \equiv \int_{-1}^{1} g(\mu)d\mu\,. \tag{3}$$

The non-negative function $F(\mu, x, t)$ is the density of particles with respect to the measure $d\mu dx$. The constant ε is a positive parameter and the variable $\sigma = \sigma(x)$ is the (scaled)

material cross-section. For fixed σ, the diffusive limit corresponds to $\varepsilon \to 0$. One can recover a dimensional version of (2) by setting $\varepsilon = 1$.

2.1 Derivation

If $F(\cdot, x, t) \in L^2(d\mu)$, then it can be expanded in terms of basis functions $\{p_n\}_{n=0}^{\infty}$ defined on $[-1, 1]$:

$$F(\mu, x, t) = \sum_{n=0}^{\infty} v_n(x, t) p_n(\mu) \,. \tag{4}$$

By truncating this expansion at some positive integer N, substituting the truncation into (2), and then taking moments with respect to $\{p_n\}_{n=0}^{N}$, one can derive a system of equations which approximates the evolution of expansion coefficients $\{v_n\}_{n=0}^{N}$. With the vector notation

$$\mathbf{p} := (p_0, p_1, \ldots, p_N)^T \quad \text{and} \quad \mathbf{v} := (v_0, v_1, \ldots, v_N)^T \,, \tag{5}$$

these equations take the form

$$\left\langle \mathbf{p}\mathbf{p}^T \right\rangle \partial_t \mathbf{v} + \frac{1}{\varepsilon} \left\langle \mu \mathbf{p}\mathbf{p}^T \right\rangle \partial_x \mathbf{v} = -\frac{\sigma}{\varepsilon^2} \left(\left\langle \mathbf{p}\mathbf{p}^T \right\rangle - \frac{1}{2} \left\langle \mathbf{p} \right\rangle \left\langle \mathbf{p} \right\rangle^T \right) \mathbf{v} \,, \tag{6}$$

or in terms of the moments $\mathbf{u} = (u_0, u_1, \ldots, u_N)^T := \langle \mathbf{p} F \rangle = \left\langle \mathbf{p}\mathbf{p}^T \right\rangle \mathbf{v}$,

$$\partial_t \mathbf{u} + \frac{1}{\varepsilon} \left\langle \mu \mathbf{p}\mathbf{p}^T \right\rangle \left\langle \mathbf{p}\mathbf{p}^T \right\rangle^{-1} \partial_x \mathbf{u} = -\frac{\sigma}{\varepsilon^2} \left(\mathbf{u} - \frac{1}{2} \left\langle \mathbf{p} \right\rangle \left\langle \mathbf{p} \right\rangle^T \left\langle \mathbf{p}\mathbf{p}^T \right\rangle^{-1} \mathbf{u} \right) \,. \tag{7}$$

In practice, the right-hand side of (7) is usually much simpler than it appears in this abstract setting.

In the P_N approximation, the basis functions in (7) are chosen to be the Legendre polynomials [1], which satisfy the orthogonality relation

$$\langle p_n p_m \rangle = \frac{2}{2n+1} \delta_{nm} \tag{8}$$

and the recursion relation

$$\mu p_n(\mu) = \frac{n+1}{2n+1} p_{n+1}(\mu) + \frac{n}{2n+1} p_{n-1}(\mu) \,, \quad \mu \in [-1, 1] \,. \tag{9}$$

The first four Legendre polynomials are

$$p_0(\mu) = 1 \,, \quad p_1(\mu) = \mu \,, \quad p_2(\mu) = \frac{1}{2} \left(3\mu^2 - 1 \right) \,, \quad p_3(\mu) = \frac{1}{2} (5\mu^3 - 3\mu) \,; \tag{10}$$

for notational convenience, we denote their corresponding moments by

$$\rho := u_0 \,, \quad m := u_1 \,, \quad w := u_2 \,, \quad q := u_3 \,. \tag{11}$$

Using (8) and (9) and the fact that $p_0 = 1$, one can evaluate the integrals in (7) to arrive at the (scaled) P_N equations

$$\partial_t \mathbf{u} + \frac{1}{\varepsilon} (A + B) \partial_x \mathbf{u} = -\frac{\sigma}{\varepsilon^2} Q \mathbf{u} \,, \tag{12}$$

where the flux matrices A and B and the relaxation matrix Q are given by

$$A_{nm} = \frac{n+1}{2n+1}\,\delta_{n+1,m}\,, \qquad B_{nm} = \frac{n}{2n+1}\delta_{n-1,m}\,, \qquad Q_{nm} = \delta_{nm}(1-\delta_{n,0})\,. \tag{13}$$

This system is linear hyperbolic. The eigenvalues of the matrix $A+B$ are the roots $\{\lambda_i\}_{i=1}^N \subset [-1,1]$ of the polynomial p_{N+1}. These roots (which are real and distinct) appear in pairs with opposite signs that accumulate at $\{\pm 1\}$ as $N \to \infty$. Corresponding to each eigenvalue λ_i is a right eigenvector $\mathbf{r}_i = \mathbf{p}(\lambda_i)$.

In practice, P_N equations are only used with odd values of N. The reason for this is that one of the eigenvalues of the matrix $A+B$ is zero when N is even. In such cases, it is not possible to specify boundary conditions that are consistent with the original transport equation [20]. Indeed, it turns out that a P_{2s} system is typically less accurate than the preceding P_{2s-1} system [7].

To provide the reader with intuition, plots of the variable ρ from a series of highly resolved P_N calculations are provided in Figure 1 for increasing values of N. The domain of this problem is the interval $[0,2]$ and the boundary conditions are periodic. The initial condition for ρ is

$$\rho(x,0) = \begin{cases} 2.0, & x \in (0.8, 1.2)\,, \\ 0.0, & x \in [0, 0.8] \cup [1.2, 2.0]\,, \end{cases} \tag{14}$$

All other moments are initially set to zero. As expected, the profile of ρ converges as N increases. In practice, the number of equations needed to obtain sufficiently accurate results decreases as collisions become more prevalent. Indeed, the P_N equations are often used in transition regimes, where the diffusion approximation of (2) is not valid but collisions still play a major role in the dynamics of the system.

The reader may also note that the support of ρ expands as N increases. As more variables are added to the system, the fastest wave speeds approach the limiting value of the transport equation. For the calculations in Figure 1, $\varepsilon = 2.0$ and $t = 1.0$. Hence the transport equation will propagate information from the initial data (14) a maximum distance of 0.5—meaning that the support of the transport solution at $t = 1.0$ is the interval $[0.3, 1.7]$.

2.2 Asymptotics and Rescaling

A formal asymptotic analysis of (12) shows that for small ε, $u_n = O(\varepsilon^n)$. We therefore rescale each component of $\mathbf{u}$ to an order one quantity: $u_n \to \varepsilon^n u_n$. With this rescaling, the expansion of F in (4) becomes

$$F = \sum_{n=0}^{N} \varepsilon^n v_n(x,t) p_n(\mu) = \sum_{n=0}^{N} \frac{2n+1}{2} \varepsilon^n u_n(x,t) p_n(\mu)\,, \tag{15}$$

while the P_N system (12) takes the form

$$\partial_t \mathbf{u} + \left(A + \frac{1}{\varepsilon^2} B\right) \partial_x \mathbf{u} = -\frac{\sigma}{\varepsilon^2} Q\mathbf{u}\,. \tag{16}$$

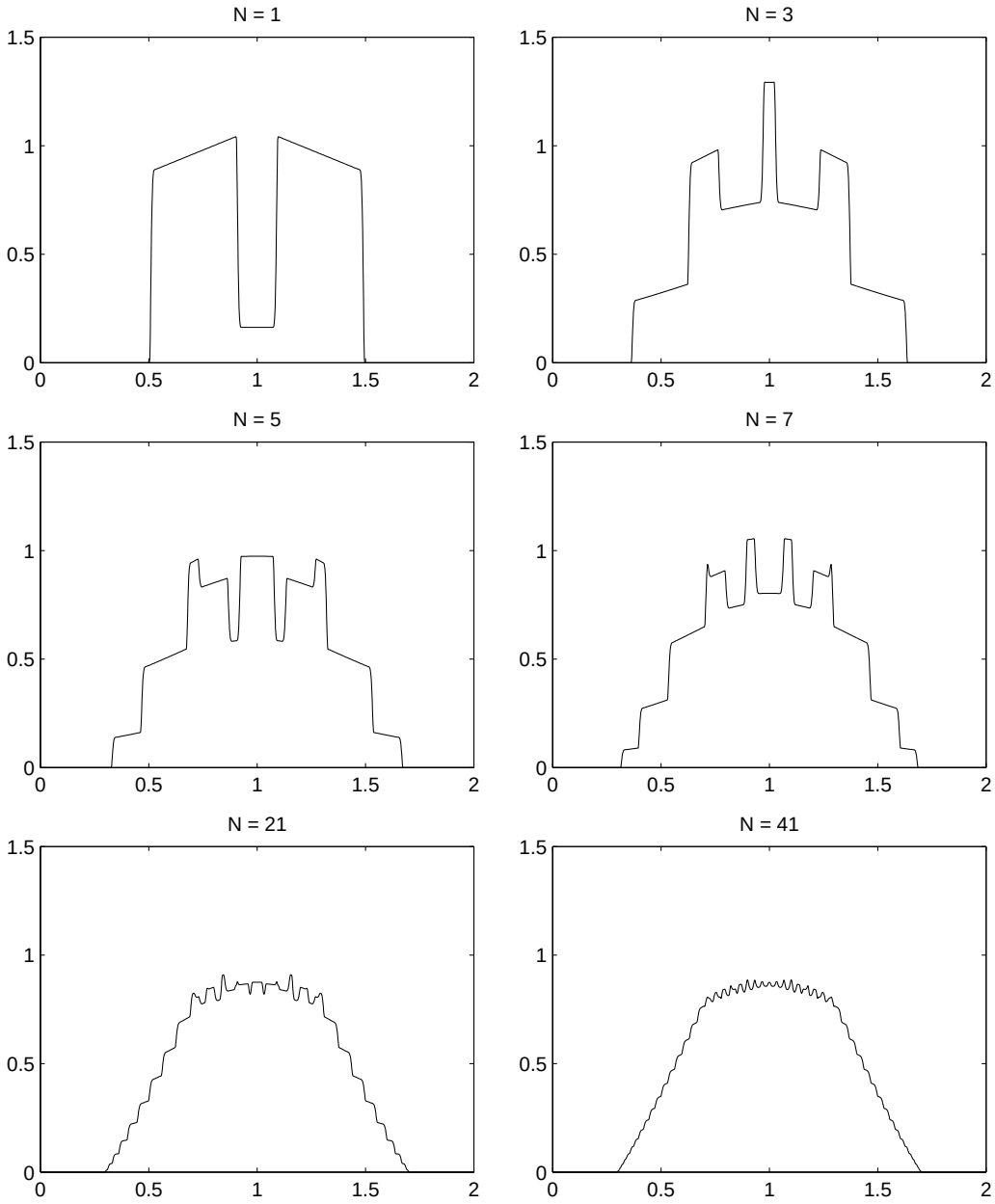

Figure 1: Comparison of ρ for $\varepsilon = 2.0$ at time $t = 1.0$ and increasing choices of N. Initial condition given by (14). In all cases, $h = 0.002$ and the computational time step is $\Delta t = 0.1h$.

This scaling is non-standard, but it makes the asymptotic analysis more transparent. *Thus, unless explicitly stated otherwise, all variables in the remainder of the paper are defined with respect to this scaling.*

One might note that the matrices A and B appear in (12) and (16) in different linear combinations, without any effect on the hyperbolicity. Given that these two systems are equivalent (modulo a change of variables), this fact should come as no surprise. However, it turns out that this is a special case of the following useful result.

Proposition 1 *For the matrices A and B defined in (13), let*

$$A + B = R\Lambda L\,, \tag{17}$$

with $L = R^{-1}$, be a diagonalization of the matrix $A + B$. Then for any $\alpha, \beta > 0$

$$\alpha A + \beta B = R^{\alpha\beta}\Lambda^{\alpha\beta}L^{\alpha\beta}\,, \tag{18}$$

with

$$\Lambda_{ii}^{\alpha\beta} = \sqrt{\alpha\beta}\Lambda_{ii}\,, \qquad R_{ij}^{\alpha\beta} = \left(\frac{\beta}{\alpha}\right)^{i/2} R_{ij}\,, \qquad L_{ij}^{\alpha\beta} = \left(\frac{\alpha}{\beta}\right)^{j/2} L_{ij}\,, \tag{19}$$

is a diagonalization of the matrix $\alpha A + \beta B$.

Proposition 1 will be used for analysis and computation throughout the paper. Its proof is a straight-forward calculation.

For fixed σ, a Chapman-Enskog analysis of (2) shows that

$$F = \frac{\rho}{2} + O(\varepsilon) \tag{20}$$

and that ρ formally satisfies the diffusion equation

$$\partial_t \rho = \partial_x \left(\frac{1}{3\sigma}\partial_x \rho\right)\,, \tag{21}$$

up to order ε^2. A similar analysis follows for the P_N equations: while (20) follows immediately from (15), equation (21) is formally established by examining the first two equations in (16):

$$\partial_t \rho + \partial_x m = 0\,, \tag{22a}$$

$$\partial_t m + \frac{1}{3}\frac{1}{\varepsilon^2}\partial_x \rho + \frac{2}{3}\partial_x w = -\frac{\sigma}{\varepsilon^2} m\,. \tag{22b}$$

For ε small, (22b) implies that $m = -\frac{1}{3\sigma}\partial_x \rho + O(\varepsilon^2)$ which, upon substitution into (22a), recovers (21).

3 The P_1 System

In this section we introduce the P_1 system and discuss the numerical challenges of simulating general P_N systems in the context of this simple example. We then present the approach taken in [14] that will serve as a starting point for our general method. The assumption that $\sigma = 1$ was used throughout [14] and, for simplicity of exposition, we maintain this assumption here and in the next section. Non-constant cross-sections will be discussed in Section 5.

The P_1 system, also known as the *hyperbolic heat equation*, is a relaxation model formulated in a simple 2×2 system:

$$\partial_t \rho + \partial_x m = 0\,, \tag{23a}$$

$$\partial_t m + \frac{1}{3}\frac{1}{\varepsilon^2}\partial_x \rho = -\frac{1}{\varepsilon^2} m\,. \tag{23b}$$

This model and nonlinear variants have been studied both theoretically [17,22,24,25,27] and numerically [11, 15, 23]. Studies of relaxation in related models can be found in the context of radiation and neutron transport [5, 12, 19, 26, 28] and also in drift-diffusion systems such as charge transport in semiconductors [13, 16, 29] and chemotaxis [8, 9].

Upon diagonalization, the P_1 system (23) takes the form of a Goldstein-Taylor model [10, 34] with wave speeds $\pm(\sqrt{3}\varepsilon)^{-1}$. Indeed, if we set $\phi^{\pm} = \rho \pm \sqrt{3}\varepsilon m$, then

$$\partial_t \phi^+ + \frac{1}{\varepsilon}\frac{1}{\sqrt{3}}\partial_x \phi^+ = -\frac{1}{2\varepsilon^2}(\phi^+ - \phi^-)\,, \tag{24a}$$

$$\partial_t \phi^- - \frac{1}{\varepsilon}\frac{1}{\sqrt{3}}\partial_x \phi^- = -\frac{1}{2\varepsilon^2}(\phi^- - \phi^+)\,. \tag{24b}$$

Meanwhile, the diffusive character of (23) is evident upon formally balancing powers of ε in (23b) to specify a closure for (23a) that is accurate up to $O(\varepsilon^2)$:

$$m = -\frac{1}{3}\partial_x \rho\,, \tag{25a}$$

$$\partial_t \rho = \frac{1}{3}\partial_x^2 \rho\,. \tag{25b}$$

3.1 Numerical Difficulties

The numerical difficulties associated with (23) have been well documented [15, 23]. For conventional schemes, there are essentially two related issues that arise in the limit $\varepsilon \to 0$. They are (i) excessive numerical dissipation and (ii) a restrictive time step. Both are easily understood by way of a semi-discrete, first-order upwind scheme for (24):

$$d_t \phi_i^+ + \frac{1}{\varepsilon}\frac{1}{\sqrt{3}}\frac{\phi_i^+ - \phi_{i-1}^+}{h} = -\frac{1}{2\varepsilon^2}(\phi_i^+ - \phi_i^-)\,, \tag{26a}$$

$$d_t \phi_i^- - \frac{1}{\varepsilon}\frac{1}{\sqrt{3}}\frac{\phi_{i+1}^- - \phi_i^-}{h} = -\frac{1}{2\varepsilon^2}(\phi_i^- - \phi_i^+)\,, \tag{26b}$$

which, in terms of ρ and m takes the form

$$\partial_t \rho_i + \frac{m_{i+1} - m_{i-1}}{2h} = \frac{h}{2\varepsilon}\frac{1}{\sqrt{3}}\frac{\rho_{i+1} - 2\rho_i + \rho_{i-1}}{h^2}\,, \tag{27a}$$

$$\partial_t m_i + \frac{1}{\varepsilon^2}\frac{1}{3}\frac{\rho_{i+1} - \rho_{i-1}}{2h} + \frac{1}{\varepsilon^2} m_i = \frac{h}{2\varepsilon}\frac{1}{\sqrt{3}}\frac{m_{i+1} - 2m_i + m_{i-1}}{h^2}\,. \tag{27b}$$

Here, and throughout the paper, h is the size of a uniform mesh spacing. For ε small, the dominant balance in (27b) is

$$m_i = -\frac{1}{3}\frac{\rho_{i+1} - \rho_{i-1}}{2h} + O(\varepsilon)\,, \tag{28}$$

which when substituted into (27a), gives

$$\partial_t \rho_i = \frac{1}{3}\frac{\rho_{i+2} - 2\rho_i + \rho_{i-2}}{4h^2} + \frac{h}{2\varepsilon}\frac{1}{\sqrt{3}}\frac{\rho_{i+1} - 2\rho_i + \rho_{i-1}}{h^2} + O(\varepsilon)\,. \tag{29}$$

As $\varepsilon \to 0$, the first term on the right hand-side of (29) yields a consistent discretization of the diffusive flux on the right-hand side of (25b). However, the second term on the right-hand side of (29)—the numerical dissipation term—will clearly affect the accuracy of the solution unless the mesh spacing h is chosen much smaller than ε—an expensive undertaking given that one need not resolve such small scales when discretizing the diffusion equation (25b) directly. The expense of resolving ε is exacerbated by a stiff hyperbolic CFL condition which requires that the time step Δt in any temporal discretization of (27) satisfies

$$\Delta t < \varepsilon C h \tag{30}$$

for some $O(1)$ constant C. Although higher-order Godunov-type schemes will decrease the dissipation in (29) with respect to h, the factor of ε^{-1} remains[1], as does the restrictive CFL condition in (30).

Many schemes have been proposed to address the problem of excessive numerical dissipation. In [15], a splitting method is proposed that separates the system in stiff and non-stiff components. This approach is also used in [14] to develop modified equations with better asymptotic properties. In [11], a well-balanced approach takes advantage of the fact that the asymptotic balance in (25a) is equivalent to the steady-state solution of (23b). In [23, 26], a discontinuous Galerkin method uses an additional variable in each computational cell to capture the diffusion limit. All of these schemes are *asymptotic preserving* (AP) [14] in the sense that they give consistent discretizations of the diffusion equation in the limit as $\varepsilon \to 0$, and most of them have an improved time step restriction $\Delta t \lesssim h^2$ in the diffusive limit that corresponds to the time step restriction for an explicit discretization of (25b). A notable exception is [5], in which a fully implicit version of the well-balanced approach from [11] is implemented for a nonlinear version of the P_1 system.

3.2 Temporal Regularization

In this subsection, we recall specifically the method found in [14], which will serve as our starting point for examining P_N systems. The key idea for this method is to regularize the P_1 system (23) via a temporal splitting of stiff and non-stiff components:

1. Stiff:

$$\partial_t \rho = 0\,, \tag{31a}$$

$$\partial_t m + \frac{1}{\varepsilon^2}\frac{1}{3}\partial_x \rho = -\frac{1}{\varepsilon^2} m\,; \tag{31b}$$

[1]For example, the dissipation term for an upwind scheme with linear, central difference reconstructions is $O(\varepsilon^{-1}h^3)$ [23].

2. Non-Stiff:

$$\partial_t \rho + \partial_x m = 0\,, \tag{31c}$$
$$\partial_t m = 0\,. \tag{31d}$$

(Actually the splitting used in [14] is a variation of (31) that gives a well-posed hyperbolic problem for the non-stiff component. This requirement is necessary for the scheme developed in [15], but it turns out not to be important for our purposes.) By applying backward Euler to the stiff component and forward Euler to the non-stiff component in (31), one arrives at the semi-discrete scheme

$$\rho^{k+1} = \rho^k - \Delta t \gamma \partial_x m^k + \frac{1}{3}\Delta t(1-\gamma)\partial_{xx}\rho^k\,, \tag{32a}$$
$$m^{k+1} = \gamma m^k - \frac{1}{3}(1-\gamma)\partial_x \rho^k\,, \tag{32b}$$

where Δt is the time step and

$$\gamma := \frac{\varepsilon^2}{\varepsilon^2 + \Delta t} \to 0 \quad \text{as} \quad \varepsilon \to 0\,. \tag{33}$$

Although derived using an implicit step, this scheme is essentially explicit, since spatial derivatives operate only at the current time step. However, it is also an $O(\Delta t)$ approximation of the continuum system

$$\partial_t \rho + \gamma \partial_x m = \frac{1}{3}(1-\gamma)\partial_{xx}\rho\,, \tag{34a}$$
$$\partial_t m + \frac{1}{3}\frac{\gamma}{\varepsilon^2}\rho_x = -\frac{\gamma}{\varepsilon^2} m\,, \tag{34b}$$

which can then be discretized with standard techniques.

We point out several important features of (34):

1. The splitting used to derive (32) is also used in [15], but in the latter case, each step is discretized in space independently. However, as noted in [14], separate spatial discretizations (i) increase computational expense and (ii) result in third order numerical derivatives with subtle stability issues. Moreover, in the limit as $\varepsilon \to 0$, the discretization of ρ becomes
$$\partial_t \rho_i = \frac{\rho_{i+2} - 2\rho_i + \rho_{i-2}}{4h^2}\,. \tag{35}$$
While this discretization is consistent with the diffusion equation (25b), it is defined on a staggered grid and thus susceptible to binary oscillations.

2. The wave speeds of the regularized P_1 system (34) are
$$\lambda_\pm = \sqrt{\frac{\gamma^2}{3\varepsilon^2}} = \frac{1}{\sqrt{3}}\frac{\varepsilon}{\varepsilon^2 + \Delta t}\,. \tag{36}$$

Thus the hyperbolic CFL condition for (34) is

$$(\varepsilon - Ch)\Delta t \leq Ch\varepsilon^2\,, \tag{37}$$

where C is an $O(1)$ constant and depends on the particular numerical scheme that is applied to (34) . For fixed ε, there are two cases: either ε is resolved by the spatial mesh ($Ch < \varepsilon$) or it is under-resolved ($Ch > \varepsilon$). In the resolved case,

$$\Delta t \leq \frac{Ch\varepsilon^2}{\varepsilon - Ch}\,, \tag{38}$$

and as $h \to 0$, we recover the original CFL condition. For fixed mesh size, one can easily check that (38) is most restrictive when $\varepsilon = 2Ch$, in which case (37) reduces to the explicit diffusive constraint $\Delta t \leq 4C^2h^2$. Any explicit discretization of the convective terms in (34a) will require this type of constraint in order to be stable for all values of ε. For the under-resolved case, (37) imposes no time restriction at all. Thus with an implicit discretization of the diffusion term on the right-hand side of (34a), the time step is determined only by temporal accuracy requirements. Although not implemented in [14], this is one of the more powerful features of the method from an applications point of view since, in many cases, an explicit diffusion condition—while better than (30)—is still too restrictive.

3. The effect of the temporal regularization is to slow down the wave speeds. However, for $\Delta t \sim h^2 \sim \varepsilon^2$,

$$|\lambda_\pm| \sim \frac{1}{h}\,. \tag{39}$$

In such cases, the numerical dissipation in a first-order upwind scheme for (34) will be $O(1)$. Therefore higher order schemes (such as the MUSCL-type scheme used in [14]) are required to ensure that the discretization of (34) is AP in all regimes. One must still accept a loss of spatial accuracy, but such losses are limited to one drop in order. In particular, for a standard Godunov-type method, $O(\varepsilon^{-1}h^\nu)$ dissipation terms in the discretization of the P_1 system become (at worst) $O(h^{\nu-1})$ terms in the discretization of the regularized system.

4 The P_3 System.

Although many schemes for the P_1 system (23) (or similar 2×2 versions thereof) have been developed, general P_N systems have received far less attention. Extending P_1 schemes to general P_N system is not always straight-forward for two reasons:

1. In general, each component u_n in (16) is coupled to the rest of the system through a flux that is a linear combination of the components u_{n+1} and u_{n-1}. The only exceptions are the first ($n = 0$) and last ($n = N$) components, which happen to be the *only* components of the P_1 system. As a result the structure of P_1 is much simpler than the general P_N system. For example, the splitting in (31) completely decouples the evolution of ρ and m into separate equations. Such decoupling does not happen for P_N when $N > 1$.

2. Many P_1 methods (including the one from [14]) are based on the idea of projecting the momentum variable m onto its leading order asymptotic value, as given in (25a). Extending this approach to general P_N leads to systems with spatial derivatives up to order N. In such cases, it is not clear whether the resulting equations are well posed and, if they are, how to handle them numerically.

We now highlight these two issues in some detail for the case $N = 3$. If we again set $\sigma = 1$ and let

$$\mathbf{u} = (\rho, m, w, q)^T \,, \tag{40}$$

then the P_3 system takes the form

$$\partial_t \rho + \partial_x m = 0 \,, \tag{41a}$$

$$\partial_t m + \partial_x \left(\frac{1}{\varepsilon^2} \frac{1}{3} \rho + \frac{2}{3} w \right) = -\frac{1}{\varepsilon^2} m \,, \tag{41b}$$

$$\partial_t w + \partial_x \left(\frac{1}{\varepsilon^2} \frac{2}{5} m + \frac{3}{5} q \right) = -\frac{1}{\varepsilon^2} w \,, \tag{41c}$$

$$\partial_t q + \partial_x \left(\frac{1}{\varepsilon^2} \frac{3}{7} w \right) = -\frac{1}{\varepsilon^2} q \,. \tag{41d}$$

The wave speeds of this system are

$$\lambda \in \left\{ \pm \frac{1}{\varepsilon} \sqrt{\frac{15 \pm 2\sqrt{30}}{35}} \right\} = \frac{1}{\varepsilon} \left\{ \pm 0.33998..., \pm 0.86114... \right\} . \tag{42}$$

We perform a Chapman-Enskog analysis for (41) by formally expanding m, w, and q in ε:

$$m = m^{(0)} + \varepsilon^2 m^{(2)} + \varepsilon^4 m^{(4)} + \dots \,, \tag{43a}$$

$$w = w^{(0)} + \varepsilon^2 w^{(2)} + \varepsilon^4 w^{(4)} + \dots \,, \tag{43b}$$

$$q = q^{(0)} + \varepsilon^2 q^{(2)} + \varepsilon^4 q^{(4)} + \dots \,, \tag{43c}$$

where $m^{(2k)}$, $w^{(2k)}$, and $q^{(2k)}$ depend on ρ and its derivatives. Substituting this expansion into (41) yields the following asymptotics:

1. Leading order (equilibrium) terms:

$$\partial_t \rho = \frac{1}{3} \partial_x^2 \rho + O(\varepsilon^2) \,, \tag{44a}$$

$$m^{(0)} = -\frac{1}{3} \partial_x \rho \,, \quad w^{(0)} = \frac{2}{15} \partial_x^2 \rho \,, \quad q^{(0)} = -\frac{2}{35} \partial_x^3 \rho \,; \tag{44b}$$

2. Order ε^2 terms:

$$\partial_t \rho = \frac{1}{3} \partial_x^2 \rho - \frac{1}{45} \varepsilon^2 \partial_x^4 \rho + O(\varepsilon^4) \,, \tag{45a}$$

$$m^{(2)} = \frac{1}{45} \partial_x^3 \rho \,, \quad w^{(2)} = -\frac{2}{105} \partial_x^4 \rho \,; \tag{45b}$$

3. Order ε^4 terms:

$$\partial_t \rho = \frac{1}{3}\partial_x^2 \rho - \frac{1}{45}\varepsilon^2 \partial_x^4 \rho + \frac{2}{945}\varepsilon^4 \partial_x^6 \rho + O(\varepsilon^6)\,, \tag{46a}$$

$$m^{(4)} = -\frac{2}{945}\partial_x^5 \rho\,. \tag{46b}$$

Note that we have only specified asymptotics of each moment in the P_3 system through orders that are consistent with the corresponding moments of the original transport equation (2). In general, the n^{th} component of $\mathbf{u}$ in the P_N system (16) will agree with the n^{th} moment of (2) up to a formal $O(\varepsilon^{2(N-n+1)})$ error, for all $n \geq 1$

4.1 Extending the P_1 Scheme

As with the P_1 equations, the P_3 system can be separated into stiff and non-stiff parts:

1. Stiff:

$$\partial_t \rho = 0\,, \tag{47a}$$

$$\partial_t m + \frac{1}{\varepsilon^2}\frac{1}{3}\partial_x \rho = -\frac{1}{\varepsilon^2} m\,, \tag{47b}$$

$$\partial_t w + \frac{1}{\varepsilon^2}\frac{2}{5}\partial_x m = -\frac{1}{\varepsilon^2} w\,, \tag{47c}$$

$$\partial_t q + \frac{1}{\varepsilon^2}\frac{3}{7}\partial_x w = -\frac{1}{\varepsilon^2} q\,; \tag{47d}$$

2. Non-Stiff:

$$\partial_t \rho + \partial_x m = 0\,, \tag{47e}$$

$$\partial_t m + \frac{2}{3}\partial_x w = 0\,, \tag{47f}$$

$$\partial_t w + \frac{3}{5}\partial_x q = 0\,, \tag{47g}$$

$$\partial_t q = 0\,. \tag{47h}$$

The stiff relaxation component in this splitting is in lower diagonal form. It can therefore be solved implicitly using the backward Euler method, giving

$$\rho^{k+1/2} = \rho^k\,, \tag{48a}$$

$$m^{k+1/2} = \gamma m^k - \frac{1}{3}(1-\gamma)\partial_x \rho^k\,, \tag{48b}$$

$$w^{k+1/2} = \gamma w^k - \frac{2}{5}\gamma(1-\gamma)\partial_x m^k + \frac{2}{15}(1-\gamma)^2 \partial_x^2 \rho^k\,, \tag{48c}$$

$$q^{k+1/2} = \gamma q^k - \frac{3}{7}\gamma(1-\gamma)\partial_x w^k + \frac{6}{35}\gamma(1-\gamma)^2 \partial_x^2 m^k - \frac{2}{35}(1-\gamma)^3 \partial_x^3 \rho^k\,. \tag{48d}$$

For the non-stiff component, an explicit step with forward Euler gives

$$\rho^{k+1} = \rho^{k+1/2} - \Delta t \partial_x m^{k+1/2}\,, \tag{49a}$$

$$m^{k+1} = m^{k+1/2} - \frac{2}{3}\Delta t \partial_x w^{k+1/2}\,, \tag{49b}$$

$$w^{k+1} = w^{k+1/2} - \frac{3}{5}\Delta t \partial_x q^{k+1/2}\,, \tag{49c}$$

$$q^{k+1} = q^{k+1/2}\,. \tag{49d}$$

Combining (48) and (49), we have

$$\rho^{k+1} = \rho^k - \Delta t\gamma\partial_x m^k + \frac{1}{3}\Delta t(1-\gamma)\partial_x^2\rho^k\,, \tag{50a}$$

$$m^{k+1} = \gamma m^k - \frac{1}{3}(1-\gamma)\partial_x\rho^k - \frac{2}{3}\Delta t\gamma\partial_x w^k + \frac{4}{15}\Delta t\gamma(1-\gamma)\partial_x^2 m^k \tag{50b}$$

$$- \frac{4}{45}\Delta t(1-\gamma)^2\partial_x^3\rho^k\,, \tag{50c}$$

$$w^{k+1} = \gamma w^k - \frac{2}{5}\gamma(1-\gamma)\partial_x m^k - \frac{3}{5}\Delta t\gamma\partial_x q^k + \frac{2}{15}(1-\gamma)^2\partial_x^2\rho^k \tag{50d}$$

$$+ \frac{9}{35}\Delta t\gamma(1-\gamma)\partial_x^2 w^k - \frac{18}{175}\Delta t\gamma(1-\gamma)^2\partial_x^3 m^k + \frac{6}{175}\Delta t\,(1-\gamma)^3\,\partial_x^4\rho^k\,, \tag{50e}$$

$$q^{k+1} = \gamma q^k - \frac{3}{7}\gamma(1-\gamma)\partial_x w^k + \frac{6}{35}\gamma(1-\gamma)^2\partial_x^2 m^k - \frac{2}{35}\,(1-\gamma)^3\,\partial_x^3\rho^k\,, \tag{50f}$$

which is an $O(\Delta t)$ approximation of the temporally regularized system

$$\partial_t\rho + \partial_x m - \frac{1}{3}(1-\gamma)\partial_x^2\rho = 0\,, \tag{51a}$$

$$\partial_t m + \partial_x\left(\frac{1}{3}\frac{\gamma}{\varepsilon^2}\rho + \frac{2}{3}\gamma w\right) - \frac{4}{15}\gamma(1-\gamma)\partial_x^2 m^n + \frac{4}{45}(1-\gamma)^2\partial_x^3\rho^n = -\frac{\gamma}{\varepsilon^2}m\,, \tag{51b}$$

$$\partial_t w + \partial_x\left(\frac{2}{5}\frac{\gamma^2}{\varepsilon^2}m + \frac{3}{5}\gamma q\right) - \frac{2}{15}\frac{\gamma(1-\gamma)}{\varepsilon^2}\partial_x^2\rho^n - \frac{9}{35}\frac{\gamma^2}{\varepsilon^2}\partial_x^2 w^n$$

$$+\frac{18}{175}\gamma(1-\gamma)^2\partial_x^3 m^n - \frac{6}{175}\,(1-\gamma)^3\,\partial_x^4\rho^n = -\frac{\gamma}{\varepsilon^2}w\,, \tag{51c}$$

$$\partial_t q + \partial_x\left(\frac{3}{7}\frac{\gamma^2}{\varepsilon^2}w\right) - \frac{6}{35}\frac{\gamma^2(1-\gamma)}{\varepsilon^2}\partial_x^2 m^n + \frac{2}{35}\frac{\gamma(1-\gamma)^2}{\varepsilon^2}\partial_x^3\rho^n = -\frac{\gamma}{\varepsilon^2}q\,. \tag{51d}$$

In this system, each component of $\mathbf{u}$ has, up to $O(\Delta t)$, the correct leading order balance—that is, when $\varepsilon \to 0$,

$$m = -\frac{1}{3}\partial_x\rho + O(\Delta t)\,, \quad w = \frac{2}{15}\partial_x^2\rho + O(\Delta t)\,, \quad q = -\frac{2}{35}\partial_x^3\rho + O(\Delta t)\,, \tag{52}$$

and ρ satisfies

$$\partial_t\rho = \frac{1}{3}\partial_x^2\rho\ . \tag{53}$$

However, because the expressions for ρ and m in (52) and (53) are only accurate to $O(\varepsilon^2)$ anyway, the leading order balances for w and q in (52) do not improve the order of accuracy

in the asymptotic expression for F in (15). Nor do they lead to higher order accuracy in the asymptotic equation for ρ. Instead, the large number of spatial derivatives in (51) is an obvious drawback that presents the following questions:

1. Is (51) formally well-posed? (Note the sign on the term $\partial_x^4 \rho$ in (51c)). If so, are there numerical approximations that are stable (for fourth derivatives) and avoid the dispersive oscillations (for third order derivatives) like those observed in simulations of the moment system in [13]?

2. How does the regularity required for solutions of (51) affect the ability of (51) to accurately approximate the original P_3 system?

3. Can one derive well-posed boundary conditions for (51) and implement them in a practical numerical scheme?

Rather than attempt to address these questions, we will instead sacrifice the correct leading order behavior of the higher order moments (at least for an initial time step) in order to achieve a more practical regularization.

Remark 2 *It is possible to update the non-stiff component in (47) implicitly by first updating q and then working upward. However, such an approach only increases the number spatial derivatives.*

4.2 A Practical Alternative

To avoid a modified system with more than two spatial derivatives, we still use the splitting in (47), but *only the source terms* in the stiff component will be updated implicitly. The flux terms are evaluated *explicitly*, thus giving:

$$\rho^{k+1/2} = \rho^k \,, \tag{54a}$$

$$m^{k+1/2} = \gamma m^k - \frac{1}{3}(1-\gamma)\partial_x \rho^k \,, \tag{54b}$$

$$w^{k+1/2} = \gamma w^k - \frac{2}{5}(1-\gamma)\partial_x m^k \,, \tag{54c}$$

$$q^{k+1/2} = \gamma q^k - \frac{3}{7}(1-\gamma)\partial_x w^k \,. \tag{54d}$$

For the P_1 system, there is no difference in our approach, since $\rho_t = 0$ in the implicit step of (31).

We now apply the same convective step as before to arrive at the semi-discrete scheme

$$\rho^{k+1} = \rho^k - \Delta t \gamma \partial_x m^k + \frac{1}{3}\Delta t(1-\gamma)\partial_x^2 \rho^k \,, \tag{55a}$$

$$m^{k+1} = \gamma m^k - \frac{1}{3}(1-\gamma)\partial_x \rho^k - \frac{2}{3}\Delta t \gamma \partial_x w^k + \frac{4}{15}\Delta t(1-\gamma)\partial_x^2 m^k \,, \tag{55b}$$

$$w^{k+1} = \gamma w^k - \frac{2}{5}(1-\gamma)\partial_x m^k - \frac{3}{5}\Delta t \gamma \partial_x q^k + \frac{9}{35}\Delta t(1-\gamma)\partial_x^2 w^k \,, \tag{55c}$$

$$q^{k+1} = \gamma q^k - \frac{3}{7}(1-\gamma)\partial_x w^k \,, \tag{55d}$$

which, in turn, is an $O(\Delta t)$ approximation to the modified system

$$\partial_t \rho + \gamma \partial_x m = \frac{1}{3}\frac{\Delta t \gamma}{\varepsilon^2}\partial_x^2 \rho^k \,, \tag{56a}$$

$$\partial_t m + \partial_x \left(\frac{1}{3}\frac{\gamma}{\varepsilon^2}\rho + \frac{2}{3}\gamma w \right) = -\frac{\gamma}{\varepsilon^2} m + \frac{4}{15}\frac{\Delta t \gamma}{\varepsilon^2}\partial_x^2 m \,, \tag{56b}$$

$$\partial_t w + \partial_x \left(\frac{2}{5}\frac{\gamma}{\varepsilon^2} m + \frac{3}{5}\gamma q \right) = -\frac{\gamma}{\varepsilon^2} w + \frac{9}{35}\frac{\Delta t \gamma}{\varepsilon^2}\partial_x^2 w \,, \tag{56c}$$

$$\partial_t q + \partial_x \left(\frac{3}{7}\frac{\gamma}{\varepsilon^2} w \right) = -\frac{\gamma}{\varepsilon^2} q \,. \tag{56d}$$

Note that in deriving (55) from (55), we have let $\Delta t \to 0$ only in evaluating time derivates. The remaining instances of Δt are held fixed.

We point out the key features of this regularized system, which we refer to as RP_3 (*regularized* P_3). The first three items are features of the P_1 scheme that we wish to maintain. The last item is a consequence of the new method applied to a larger ($N > 1$) system.

1. According to Proposition 1, the RP_3 system is hyperbolic with waves speeds of the order

$$\sqrt{\frac{\gamma}{\varepsilon}} = \frac{\varepsilon}{\varepsilon^2 + \Delta t} \,. \tag{57}$$

   This implies a hyperbolic time step restriction given by (38). Moreover, $O(h^\nu/\varepsilon)$ dissipation terms in a Godunov-type discretization of the P_3 system are replaced by terms that are $O(h^{\nu-1})$ or smaller.

2. For under-resolved cases ($\varepsilon < Ch$), there is no hyperbolic time step restriction. Thus an implicit discretization of the diffusive terms in (56) leads to schemes for which the time step is based only on requirements of temporal accuracy. In this respect, an attractive feature of the regularized system is that there is no coupling of components through the diffusive terms.

3. As $\varepsilon \to 0$, $\gamma \to 0$ so that (56a) recovers the diffusion equation (44a) for ρ at leading order. Moreover, because the diffusion term in (56a) is built into the equation, any spatial discretization will inherit the same property.

4. The price of implementing (56) instead of (51) is that the terms w and q in (56) do not possess the correct leading order balance (see (44)) after a single time step. Instead, in the limit as $\varepsilon \to 0$,

$$w^{k+1} = -\frac{2}{5}\partial_x m^k + O(\Delta t) \,, \tag{58a}$$

$$q^{k+1} = -\frac{3}{7}\partial_x w^k + O(\Delta t) \,. \tag{58b}$$

   If m^k and w^k have the correct leading order balance, then so will q^{k+1} and w^{k+1}. However, this will not be the case for general initial data. Even so, the correct balance *will* be achieved after three time steps. In the first time step, m^{k+1} is projected into

its equilibrium value. Then w^{k+2} is projected into its equilibrium value in the next step and q^{k+3} is projected in the third time step. We note also that for small values of ε, the error introduced by (58a) and (58b) into the expansion (15) and the diffusion equation (44a) is $O(\varepsilon^2)$.

4.3 Numerical Examples

For numerical calculations, we introduce a spatial discretization of (56) using an explicit, conservative discretization of the convective terms and the canonical implicit discretization of the diffusive terms. In vector notation, the scheme takes the form

$$\mathbf{u}_j^{k+1} = \mathbf{u}_j^k - \Delta t M \frac{\mathbf{u}_{j+1/2}^k - \mathbf{u}_{j-1/2}^k}{h} - \frac{\Delta t \gamma}{\varepsilon^2} Q \mathbf{u}_j^k + \frac{\Delta t^2 \gamma}{\varepsilon^2} AB \frac{\mathbf{u}_{j+1}^{k+1} - 2\mathbf{u}_j^{k+1} + \mathbf{u}_{j-1}^{k+1}}{h^2}, \tag{59}$$

where $M := \gamma(\varepsilon^{-2}B + A)$ and $\mathbf{u}_j^k$ is the average of $\mathbf{u}$ at time $t_k = k\Delta t$ over a cell I_j of uniform width h. The edge fluxes $M\mathbf{u}_{j\pm1/2}^k$ in (59) are determined using a second order upwind method:

$$M\mathbf{u}_{j+1/2}^k = \frac{1}{2} M \left(\mathbf{u}_{j+1/2}^{k,l} + \mathbf{u}_{j+1/2}^{k,r} \right) + \frac{1}{2} |M| \left(\mathbf{u}_{j+1/2}^{k,l} - \mathbf{u}_{j+1/2}^{k,r} \right), \tag{60}$$

where the matrix $|M| := R|\Lambda|R^{-1}$ is calculated using the eigenvectors and eigenvalues from the diagonalization $M = R\Lambda R^{-1}$ of the matrix M. The right and left edge values of $\mathbf{u}$ in (60) are given by

$$\mathbf{u}_{j+1/2}^{k,l} = R\mathbf{w}_{j+1/2}^{k,l} \qquad \text{and} \qquad \mathbf{u}_{j+1/2}^{k,r} = R\mathbf{w}_{j+1/2}^{k,r}, \tag{61}$$

and the characteristic edge values are determined by linear reconstructions on adjacent cells:

$$\mathbf{w}_{j+1/2}^{k,l} = \mathbf{w}_j^k + \frac{h}{2}\mathbf{w}_j' \qquad \text{and} \qquad \mathbf{w}_{j+1/2}^{k,r} = \mathbf{w}_{j+1}^k - \frac{h}{2}\mathbf{w}_{j+1}', \tag{62}$$

where $\mathbf{w}_j^k := R^{-1}\mathbf{u}_j^k$ and the slopes $\mathbf{w}_j'$ approximate derivatives in each cell.

Our first calculation is an accuracy test using smooth initial data on the domain $[0, 2]$:

$$\rho(x, 0) = 1.0 + 0.9\cos(4\pi(x - 1)), \tag{63a}$$

$$m(x, 0) = w(x, 0) = q(x, 0) = 0. \tag{63b}$$

The boundary conditions are periodic. We run the RP_3 computation to times $t = 1.0$ and $t = 0.1$ for $\varepsilon = 2.0$ and $\varepsilon = 10^{-3}$, respectively. No limiter is used in the slope approximation of $\mathbf{w}'$. Convergence results are presented in Tables 1 and 2. The reader should note that the large jump in the order of converge between the 640 and 1280 point grids in Table 2 occurs when the mesh switches from under-resolved to resolved and the explicit diffusion time step restriction, as in (38), must be enforced. As a result, the time step drops from 1.25×10^{-3} to 1.67×10^{-6}.

A more interesting example uses the same boundary and initial conditions, except that

$$\rho(x, 0) = \begin{cases} 2.0, & x \in (0.8, 1.2), \\ 0.0, & x \in [0, 0.8] \cup [1.2, 2.0]. \end{cases} \tag{64}$$

	points	ρ		m		w		q	
L^2	10	9.40e-02	—	4.08e-02	—	2.25e-03	—	1.16e-04	—
	20	3.9e-02	1.25	3.89e-03	3.39	1.34e-03	0.75	1.86e-04	-0.68
	40	9.23e-03	2.10	5.95e-04	2.71	2.42e-04	2.47	2.44e-05	2.93
	80	2.28e-03	2.02	3.20e-04	0.89	4.35e-06	5.80	3.91e-06	2.64
	160	7.16e-04	1.67	9.43e-05	1.76	2.67e-05	-2.62	4.59e-06	-0.23
	320	2.66e-04	1.43	2.37e-05	1.99	1.72e-05	0.64	2.60e-06	0.82
	640	9.90e-05	1.43	5.59e-06	2.09	8.23e-06	1.06	1.19e-06	1.13
	1280	2.66e-05	1.89	1.49e-06	1.91	2.85e-06	1.53	4.06e-07	1.55
L^∞	10	1.33e-01	—	5.49e-02	—	3.19e-03	—	1.55e-04	—
	20	5.58e-02	1.25	5.23e-03	3.39	1.89e-03	0.75	2.50e-04	-0.68
	40	1.24e-02	2.17	8.42e-04	2.63	3.25e-04	2.54	3.45e-05	2.86
	80	3.19e-03	1.96	4.74e-04	0.91	6.07e-06	5.74	5.46e-06	2.66
	160	1.01e-03	1.66	1.33e-04	1.75	3.77e-05	-2.63	6.47e-06	-0.25
	320	3.77e-04	1.42	3.35e-05	1.98	2.43e-05	0.63	3.67e-06	0.82
	640	1.41e-04	1.42	7.90e-06	2.09	1.16e-05	1.06	1.68e-06	1.13
	1280	3.85e-05	1.87	2.11e-06	1.91	4.03e-06	1.53	5.74e-07	1.55

Table 1: Errors and convergence rates for the RP_3 moments with respect to an 'exact' solution computed with 1600 points. Here $t = 1.0$, $\varepsilon = 2.0$, and smooth initial data is given in (63).

	points	ρ		m		w		q	
L^2	10	1.12e-01	—	2.49-01	—	1.32e+02	—	2.39e+02	—
	20	3.76e-02	1.58	1.93e-01	0.37	1.44e+01	3.20	5.16e+02	-1.11
	40	1.57e-02	1.26	7.68e-02	1.33	1.33e+00	3.44	2.47e+01	4.39
	80	6.24e-03	1.33	2.94e-02	1.38	2.23e-01	2.57	2.49e+00	3.31
	160	2.70e-03	1.21	1.25e-02	1.24	7.38e-02	1.60	6.31e-01	1.98
	320	1.25e-03	1.12	5.68e-03	1.13	3.17e-02	1.22	2.45e-01	1.36
	640	5.97e-04	1.06	2.70e-03	1.07	2.48e-02	1.09	1.10e-01	1.15
	1280	6.73e-07	9.79	1.68e-06	10.65	2.66e-05	9.12	5.41e-03	4.35
L^∞	10	1.59e-01	—	3.35-01	—	1.87e+02	—	3.22e+02	—
	20	5.31e-02	1.58	2.60e-01	0.37	2.04e+01	3.20	6.94e+02	-1.11
	40	2.11e-02	1.33	1.09e-02	1.26	1.78e+00	3.51	3.49e+01	4.31
	80	8.71e-03	1.27	1.76e-02	1.40	3.12e-01	2.52	3.48e+00	3.33
	160	3.81e-03	1.19	1.76e-02	1.22	1.04e-01	1.58	8.89-01	1.97
	320	1.77e-03	1.11	8.03e-03	1.13	4.48e-02	1.22	3.46e-01	1.36
	640	8.85e-04	1.06	3.82e-03	1.07	2.10e-02	1.09	1.56e-01	1.15
	1280	2.50e-06	8.40	4.09e-06	9.87	6.07e-04	5.11	1.12e-03	0.48

Table 2: Errors and convergence rates for the RP_3 moments with respect to an 'exact' solution computed with 2560 points. Here $t = 0.1$, $\varepsilon = 10^{-3}$, and smooth initial data is given in (63).

For this discontinuous initial condition, we compute solutions using the upwind discretization (59) for $\varepsilon \in \{2.0, 10^{-2}, 10^{-4}\}$. For $\varepsilon = 2.0$, we calculate $\mathbf{w}_j'$ in (62) using a minmod-type limiter:

$$\mathbf{w}_j' = \frac{1}{h}\,\text{minmod}\left(\frac{1}{2}(\mathbf{w}_{j+1} - \mathbf{w}_{j-1}), \theta(\mathbf{w}_{j+1} - \mathbf{w}_j), \theta(\mathbf{w}_j - \mathbf{w}_{j-1})\right) \tag{65}$$

that is applied component-wise with $\theta = 2.0$. However, in diffusive regimes, we have observed that limiting creates small glitches near extrema due to clipping. These glitches vanish under mesh refinement and appear only in higher order moments. Other limiters—including (65) with $\theta = 1$, the Van Leer limiter, and the superbee limiter—produce similar effects. In order to avoid discrepancies due to the choice of reconstruction, we have opted to remove the limiter for $\varepsilon = 10^{-2}$ and $\varepsilon = 10^{-4}$, where the solution is presumably smooth. An in-depth analysis of limiter effects is on-going.

Results of our computations are given in Figures (2)-(4). In Figure (2), we compare P_3 and RP_3 with $\varepsilon = 2.0$ using a "coarse" mesh ($h = 0.02$) and a "fine" mesh ($h = 0.002$). The numerical results for the two systems are nearly identical for all four moments. This is to be expected since ε is resolved by both schemes on both meshes.

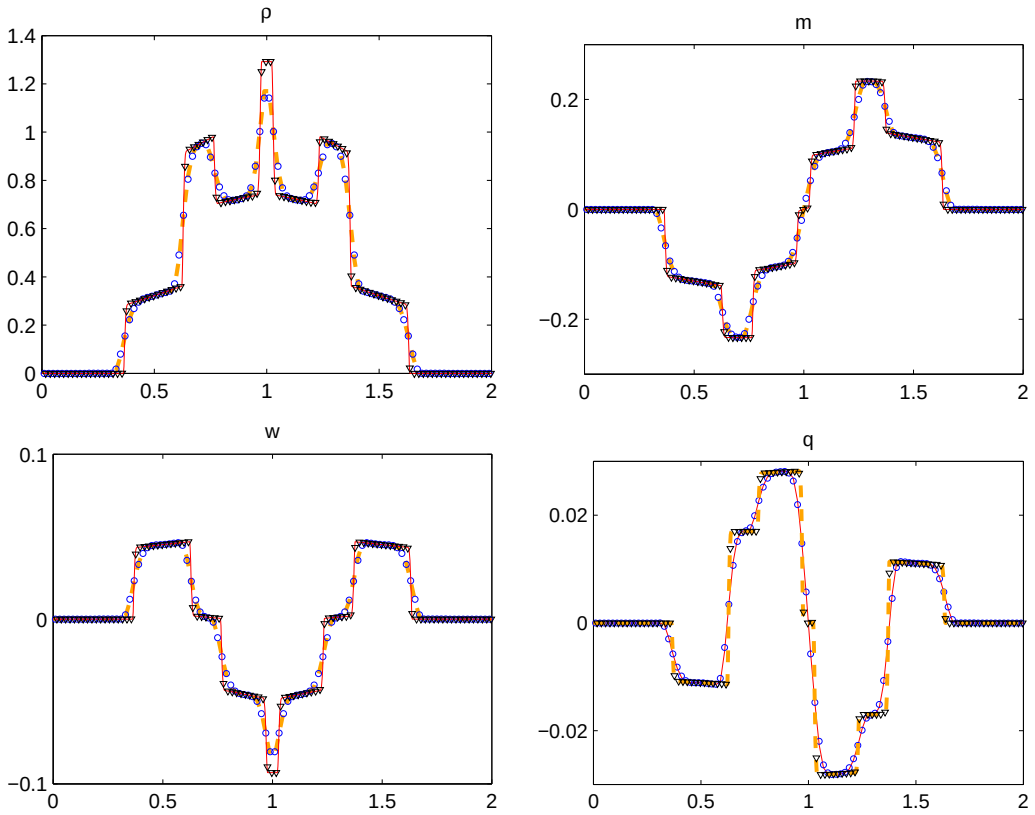

Figure 2: Comparison of P_3 and RP_3 results for $\varepsilon = 2.0$ at time $t = 1.0$. Initial condition for ρ is given by (64), while all other moments are initially zero. Dashed line: P_3, $h = 0.02$; Solid line: P_3, $h = 0.002$; circles: RP_3, $h = 0.02$; triangles: RP_3, $h = 0.002$. In all cases, the computational time step is $\Delta t = 0.1h$.

In Figure (3), we present similar results for $\varepsilon = 10^{-2}$ and $t = 0.1$. In this case, the coarse mesh almost resolves ε, and the time step for the RP_3 calculation is about 25% larger than for the P_3 calculation. For the finer mesh, ε is resolved, and the time steps are essentially the same. The results for all four computations (both systems at both resolutions) are quite similar to each other and to the leading order diffusion limit. The coarse P_3 calculation shows some discrepancies in the higher moments. However, in practice, the effect of these discrepancies is small. Indeed these differences have been over-emphasized by our choice of scaling (see Section 2.2), which has elevated all components of $\mathbf{u}$ to $O(1)$ quantities with respect to ε. For example, q only contributes to the expansion of F in (15) at order $\varepsilon^3 = 10^{-6}$.

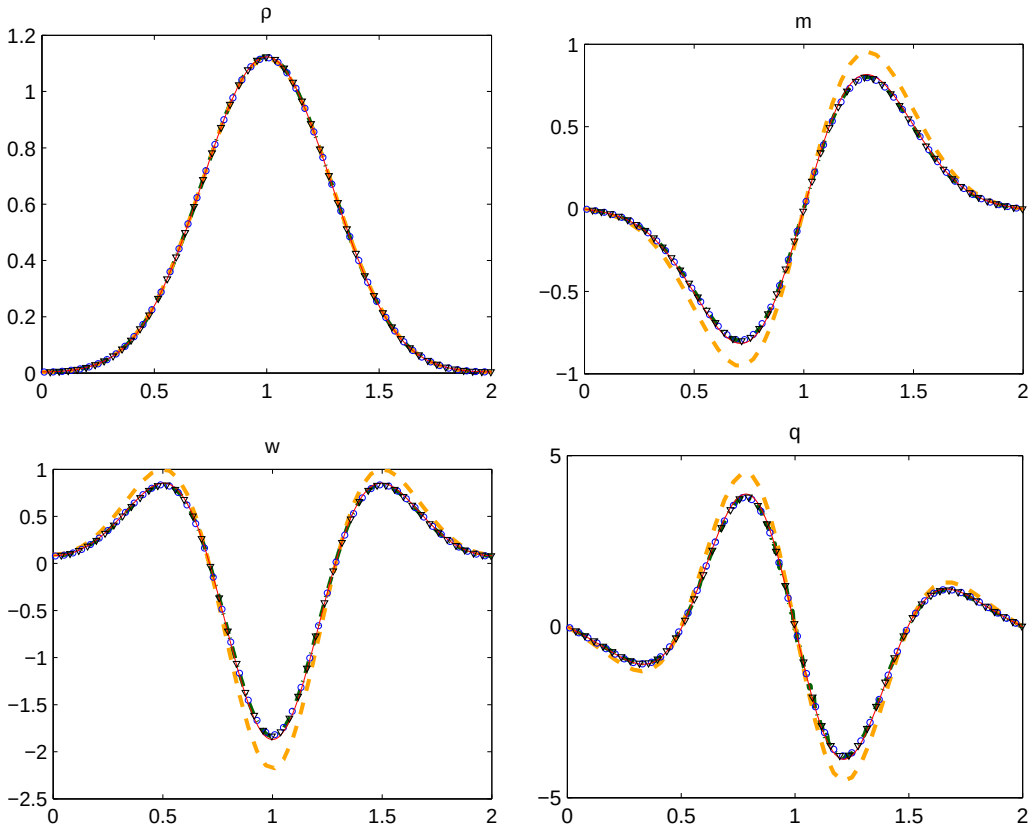

Figure 3: Comparison of P_3 and RP_3 for $\varepsilon = 10^{-2}$ and the leading order diffusion limit (52) at time $t = 0.1$. Initial condition for ρ is given by (64), while all other moments are initially zero. Dashed line: P_3, $h = 0.02$, $\Delta t = 2.0 \times 10^{-5}$; Solid line: P_3, $h = 0.002$, $\Delta t = 2.0 \times 10^{-6}$; circles: RP_3, $h = 0.02$, $\Delta t = 2.5 \times 10^{-5}$; triangles: RP_3, $h = 0.002$, $\Delta t = 2.0 \times 10^{-6}$. The solution for the diffusion limit is also given by a dash-dot line, but is not visible because of overlap.

In Figure 4, $\varepsilon = 10^{-4}$ is not resolved by either mesh. The profile of ρ computed with the P_3 system is correct at the finer mesh, because of the second-order spatial accuracy. However, the coarse mesh profile is clearly not accurate. One the other hand, the RP_3 profile for ρ—which uses a much larger time step—agrees quite closely, at both resolutions, with the solution of the diffusion equation (44a). As before, the P_3 profile for higher-order moments show noticeable discrepancies from the diffusion limit. However, because ε if so

small, these differences do not substantially contribute to the expansion of F or the closure equation for ρ.

The main point to take away from the last two figures is that as ε becomes smaller, the upwind method for P_3 requires an increasing number number of computational cells needed to maintain accuracy. Moreover, more cells means smaller time steps. Meanwhile, the RP_3 calculation will continue to capture the correct diffusion limit at a resolution that is independent of ε.

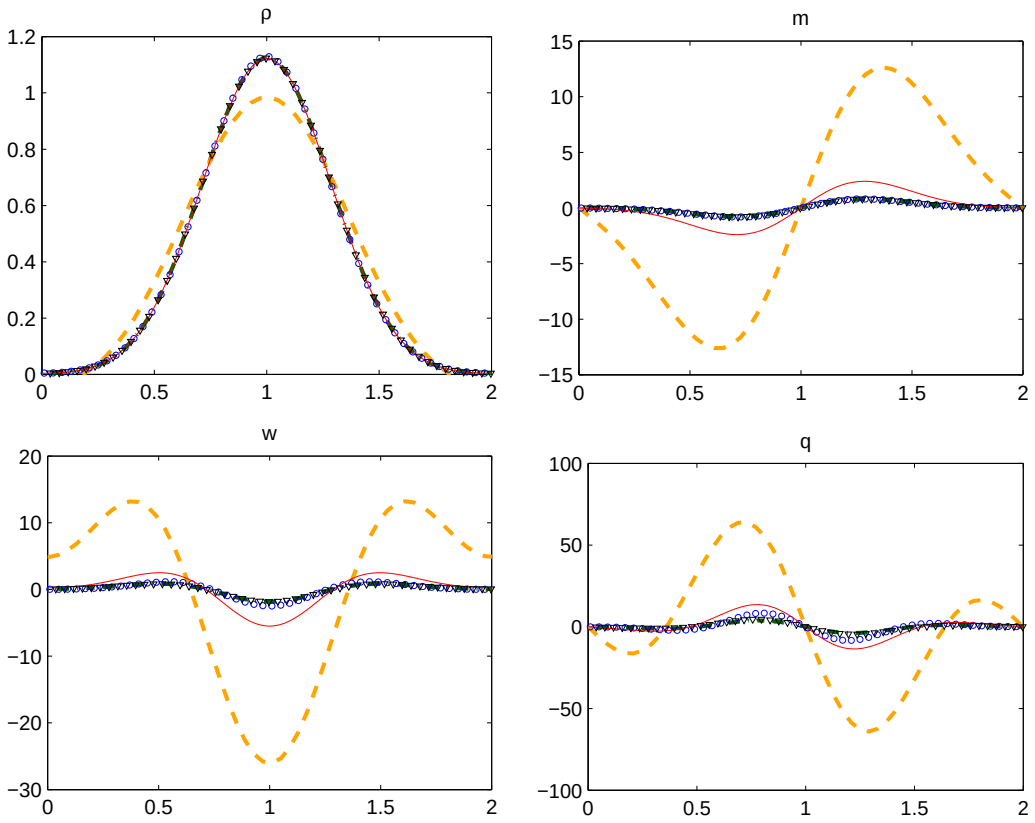

Figure 4: Comparison of P_3 and RP_3 for $\varepsilon = 10^{-4}$ and the leading order diffusion limit (52) at time $t = 0.1$. Initial condition for ρ is given by (64), while all other moments are initially zero. Dashed line: P_3, $h = 0.02$, $\Delta t = 2.0 \times 10^{-7}$; Solid line: P_3, $h = 0.002$, $\Delta t = 2.0 \times 10^{-8}$; circles: RP_3, $h = 0.02$, $\Delta t = 2.5 \times 10^{-3}$; triangles: RP_3, $h = 0.002$, $\Delta t = 2.0 \times 10^{-4}$. The solution for the diffusion limit is also given by a dash-dot line, but is not visible because of overlap.

5 General P_N Systems with Varying Cross-Sections

In this section, we apply our regularization method to general P_N systems ($N \geq 1$ and odd) with spatially varying cross-sections. The resulting regularization is a hyperbolic, non-conservative system with spatially varying fluxes and coefficients. Our numerical scheme for this system is based on the wave-splitting method in [3].

The derivation of a general regularized system uses the same recipe as before. We split the original P_N system (16) into a stiff relaxation step and a non-stiff convection step:

1. Relaxation
$$\partial_t \mathbf{u} + \frac{1}{\varepsilon^2} B \partial_x \mathbf{u} = -\frac{\sigma}{\varepsilon^2} Q \mathbf{u} \,, \tag{66a}$$

2. Convection
$$\partial_t \mathbf{u} + A \partial_x \mathbf{u} = 0 \,. \tag{66b}$$

In the relaxation step, we update the source terms implicitly and the flux terms explicitly. This gives an intermediate value

$$\mathbf{u}^{k+1/2} = \Gamma \mathbf{u}^k + \frac{\Delta t}{\varepsilon^2} \Gamma B \partial_x \mathbf{u}^k \,, \tag{67}$$

where Γ is a diagonal matrix with components

$$\Gamma_{11} = 1 \qquad \text{and} \qquad \Gamma_{nn} = \gamma := \frac{\varepsilon^2}{\varepsilon^2 + \sigma \Delta t} \,, \quad n > 1 \,. \tag{68}$$

(Note that the definition of γ above recovers the original definition (33) when $\sigma = 1$.) Applying the convection step (66b) with initial condition $\mathbf{u}^{k+1/2}$ gives

$$\begin{aligned} \mathbf{u}^{k+1} &= \mathbf{u}^{k+1/2} - \Delta t A \partial_x \mathbf{u}^{k+1/2} \\ &= \Gamma \mathbf{u}^k - \Delta t \left(A \partial_x (\gamma \mathbf{u}^k) + \frac{\gamma}{\varepsilon^2} B \partial_x \mathbf{u}^k \right) + \frac{\Delta t^2}{\varepsilon^2} A B \partial_x (\gamma \partial_x \mathbf{u}^k) \,. \end{aligned} \tag{69}$$

Here we have used the fact that, due to the special form of A and B (see (13)),

$$A\Gamma = \gamma A \qquad \text{and} \qquad \Gamma B = \gamma B \,. \tag{70}$$

The temporal discretization (69) is an $O(\Delta t)$ approximation of the *regularized* P_N, or RP_N, system

$$\partial_t \mathbf{u} + \frac{\gamma}{\varepsilon^2} B \partial_x \mathbf{u} + A \partial_x (\gamma \mathbf{u}) = -\frac{\gamma \sigma}{\varepsilon^2} Q \mathbf{u} + \frac{1}{\varepsilon^2} A B \partial_x (\Delta t \gamma \partial_x \mathbf{u}) \,. \tag{71}$$

Like the RP_3 system (56), the RP_N system has the following properties:

1. The order of the wave speeds is
$$\frac{\gamma}{\varepsilon} = \frac{\varepsilon}{\varepsilon^2 + \sigma \Delta t} \,. \tag{72}$$

   Thus the hyperbolic CFL condition is
$$(\varepsilon - Ch\sigma)\Delta t \le Ch\varepsilon^2 \,, \quad C = O(1) \,, \tag{73}$$

   and $O(h^\nu/\varepsilon)$ dissipation terms in a Godunov-type scheme for the original P_N system are now at most $O(h^{\nu-1})$.

2. When ε is under-resolved ($\varepsilon < Ch\sigma$), there is no hyperbolic time step restriction. In such cases, an implicit discretization of the diffusion term in (71) leads to a scheme for which no restriction on the time step is required for linear stability. Because the matrix AB is diagonal, solving the diffusion terms implicitly is relatively simple.

3. The equation for ρ in (71),

$$\partial_t \rho + \partial_x(\gamma m) = \frac{1}{\varepsilon^2}\frac{\Delta t}{3}\partial_x(\gamma \partial_x \rho)\,, \tag{74}$$

formally recovers the diffusion equation (21) in the limit as $\varepsilon \to 0$.

4. For $i > 1$ and fixed σ, m has the correct leading-order balance up to an $O(\Delta t)$ correction. Although the balance for higher order moments is not correct after a single time step, these moments will be projected into the correct leading order balance (up to an $O(\Delta t)$ error) after a finite number of time steps. In any event, the contribution of these terms to the asymptotic expansion of F in (15) is small when ε is small.

5.1 Spatial Discretization

Discretizing (71) in space is challenging when the cross-section varies, especially since one of the convection terms is non-conservative. We utilize the wave-splitting technique from [3], which was developed to solve hyperbolic systems with spatially varying fluxes. The wave-splitting method can also be applied to systems with source terms, which are directly incorporated into the Riemann solver. The idea of balancing fluxes and source terms in this way has been advocated in [32] in the context of Euler equations and also in [33] in a more general context. The general notion of upwinding source terms has also been a basic building block for the numerical schemes found in [2, 4, 9].

To use the wave-splitting technique, we first apply Leibniz rule to the term $\gamma B\partial_x(\mathbf{u}^k)$ and rewrite (71) in conservation form:

$$\partial_t \mathbf{u} + \left(A + \frac{1}{\varepsilon^2}B\right)\partial_x(\gamma \mathbf{u}) = -\frac{\gamma\sigma}{\varepsilon^2}Q\mathbf{u} + \frac{\Delta t}{\varepsilon^2}AB\partial_x\left(\gamma\partial_x \mathbf{u}\right) + \frac{1}{\varepsilon^2}B(\partial_x\gamma)\mathbf{u}\,. \tag{75}$$

This re-formulation ensures that the discretization of (74) will be conservative by isolating the non-conservative term $B(\partial_x\gamma)\mathbf{u}$ on the right-hand side. The trade-off is that, for higher moments of $\mathbf{u}$, we must properly interpret, even when the cross-section is discontinuous in space.

Following the recipe in [3] (but using different notation), we introduce, at each time level k and each cell interface $x_{j+1/2}$, the quantity

$$\mathbf{\Delta}^k_{j+1/2} := \left(A + \frac{1}{\varepsilon^2}B\right)(\gamma_{j+1}\mathbf{u}^k_{j+1} - \gamma_j\mathbf{u}^k_j) + \frac{\gamma_{j+1/2}\sigma_{j+1/2}}{\varepsilon^2}Q\mathbf{u}^k_{j+1/2} - \frac{1}{2\varepsilon^2}B(\gamma_{j+1}-\gamma_j)(\mathbf{u}^k_{j+1}+\mathbf{u}^k_j)\,, \tag{76}$$

which is a first order (in space) approximation of the jump across the interface due to flux differences, the source term $\varepsilon^{-2}\gamma\sigma Q\mathbf{u}^k$, and the cross-section gradient term $\varepsilon^{-2}B(\partial_x\gamma)\mathbf{u}^k$ at

time level k. The discretization of the source term at the cell interface is based on an average of adjacent cell values:

$$\gamma_{j+1/2}\sigma_{j+1/2}Q\mathbf{u}^k_{j+1/2} = \frac{1}{2}(\gamma_j\sigma_j Q\mathbf{u}^k_{j+1} + \gamma_j\sigma_j Q\mathbf{u}^k_{j+1})\,. \tag{77}$$

We then update $\mathbf{u}$ as follows:

$$\begin{aligned}\mathbf{u}^{k+1}_j = \mathbf{u}^k_j - \frac{\Delta t}{h}\left(R^-_\varepsilon L^-_\varepsilon \mathbf{\Delta}^k_{j+1/2} + R^+_\varepsilon L^+_\varepsilon \mathbf{\Delta}^k_{j-1/2}\right)\\ + \frac{\Delta t^2}{\varepsilon^2 h}AB\left((\gamma\partial_x\mathbf{u})^{k+1}_{j+1/2} - (\gamma\partial_x\mathbf{u})^{k+1}_{j-1/2}\right)\,.\end{aligned} \tag{78}$$

Here $R^\pm_\varepsilon$ and $L^\pm_\varepsilon$ are matrices of size $(N+1)\times(N+1)/2$ and $(N+1)/2\times(N+1)$, respectively, which contain the left and right eigenvectors corresponding to positive and negative eigenvalues of the matrix $\gamma(A+\varepsilon^{-2}B)$. With an appropriate scaling, these matrices can be chosen so that they are independent of γ and therefore constant in space. The diffusive fluxes in (78) are given by

$$(\gamma\partial_x\mathbf{u})_{j+1/2} = \gamma_{j+1/2}\frac{\mathbf{u}_{j+1}-\mathbf{u}_j}{h}\,, \tag{79}$$

where $\gamma_{j+1/2}$ is the harmonic average of cell values to the right and left of the interface.

A second order version of this wave-splitting scheme is also derived in [3] based on a Taylor expansion analysis. Since our current regularization is only an $O(\Delta t)$ accurate approximation of the original P_N system, we only include flux corrections to improve spatial accuracy:

$$\begin{aligned}\mathbf{u}^{k+1} = \mathbf{u}^k - \frac{\Delta t}{h}\left(R^-_\varepsilon L^-_\varepsilon \mathbf{\Delta}^k_{j+1/2} + R^+_\varepsilon L^+_\varepsilon \mathbf{\Delta}^k_{j-1/2}\right)\\ - \frac{\Delta t}{h}\left(\tilde{F}_{j+1/2} - \tilde{F}_{j-1/2}\right) + \frac{\Delta t^2}{\varepsilon^2 h}AB\left((\gamma\partial_x\mathbf{u})^{k+1}_{j+1/2} - (\gamma\partial_x\mathbf{u})^{k+1}_{j-1/2}\right)\,,\end{aligned} \tag{80}$$

where, following [3], the flux corrections are given by

$$\tilde{F}_{j+1/2} = \frac{1}{2}\sum_{n=0}^{N}\mathrm{sgn}(\lambda^n_{j+1/2})\left(1-\frac{\Delta t}{h}|\lambda^n_{j+1/2}|\right)\mathcal{L}\left\{\mathbf{r}^n_\varepsilon(\mathbf{l}^n_\varepsilon)^T\mathbf{\Delta}^k_{j+1/2}\right\}\,. \tag{81}$$

Here $\{\lambda^n_{j+1/2}\}_{n=0}^N$ are the eigenvalues of the matrix $\gamma(A+\varepsilon^{-2}B)$ evaluated on the upwind side of the cell interface, and the vectors $\{\mathbf{r}^\mathbf{n}_\varepsilon\}_{n=0}^N$ and $\{\mathbf{l}^\mathbf{n}_\varepsilon\}_{n=0}^N$ are the right and left eigenvectors of this matrix (which are constant in space). The operator $\mathcal{L}$ is a limiter given by [18]

$$\mathcal{L}(\mathbf{q}_{j+1/2}) := \phi\left(\frac{|\mathbf{q}_{j+1/2}|}{|\mathbf{q}_{j'+1/2}|}\right)\mathbf{q}_{j+1/2} \tag{82}$$

for some choice of smoothness indicator ϕ, and j' is the index on the upwind side of the interface $x_{j+1/2}$. Note that without the source term, (80) is just a limited Lax-Wendroff scheme for the left-hand side of (75).

Unfortunately, the addition of flux corrections to our scheme is not always stable. In streaming regimes, the only limiter that is consistently stable is the minmod limiter $\phi(\theta) = \text{minmod}(1, \theta)$. Worse yet, in diffusive regimes, there are cases when our implementation of (80) is unstable for the minmod limiter as well, even when the cross-section varies smoothly. Numerical experiments show that the onset of instability is marked by negative values for the variable ρ which, by definition, is a non-negative quantity. It is almost certain that the source of this instability is the naive treatment of the non-conservative term in (71), and further analysis is clearly needed here. Even so, the results of the next section clearly indicate the potential of the regularization method.

5.2 Numerical Examples

In this subsection, we revisit the example of Section (4.3), but now with spatially varying cross-sections.

5.2.1 Vanishing Cross-section

In this experiment, we set $\varepsilon = 10^{-3}$ and consider the smoothly varying cross-section

$$\sigma(x) = 100(x-1)^4\,, \tag{83}$$

which is large at the edges of the domain but vanishes in the center. The vanishing cross-section means that both the P_N and RP_N systems behave like wave equations with $O(1/\varepsilon)$ wave speeds near $x = 1$. Thus both systems are numerically stiff.

The vanishing cross-section (83) has been considered for a nonlinear version of the P_1 system in [5]. In that work, a fully implicit scheme was used in order to overcome the fast wave speeds in the center of the domain. In some applications, this approach may be preferred. However, one must be willing to sacrifice resolution of the hyperbolic wave structures in order to take time steps beyond the hyperbolic CFL condition.

The vanishing cross-section presents difficulties for Godunov-type discretizations of the RP_N system. For *global* stability, the CFL condition (73) must be satisfied for all values of σ. In particular, enforcing (73) in the center of the domain—where $\sigma = 0$ and the dynamics are *not* diffusive—requires that $\Delta t \leq Ch\varepsilon$. This small time step does not provide enough of a regularizing effect in regions of the domain where there the dynamics are diffusive, particularly in cases where $h = O(\varepsilon)$. For example, setting $\Delta t = Ch\varepsilon$ and $h = \varepsilon$ in (72) gives wave speeds on the order of

$$\frac{\gamma}{\varepsilon} = \frac{\varepsilon}{\varepsilon^2 + C\sigma\varepsilon^2} = \frac{1}{\varepsilon}\left(\frac{1}{1+C\sigma}\right)\,. \tag{84}$$

Thus when $C\sigma = O(1)$, the reduction in wave speeds is insignificant so that excessive numerical dissipation is again an issue.

One approach to solving this problem is to use a local time step to derive the regularized system (71) and then set the computational time step Δt for global stability. For the wave-splitting algorithm, this is not necessary because of the balance between sources and fluxes that is built into the solver. Indeed, we note the following

Proposition 3 *The wave splitting algorithm for the original P_N system* (16) *is asymptotic preserving.*

Note that, in this context, the original P_N systems corresponds to the extreme case $\Delta t \to 0$ in the regularized system (71). A proof of this proposition is given in the appendix.

Proposition 3 shows that the wave-splitting algorithm is an attractive option for the vanishing cross-section problem, independent of the regularization. However, it is not the best choice for generic problems because it is numerically stiff, even when $\sigma = O(1)$. A related algorithm for the P_1 system is presented in [11] that does allow for an explicit diffusive time step.

We present computational results for RP_7 computations in Figure (5) at two different resolutions, using the simple wave-splitting scheme (78) in both cases. As a reference, we compare to a profile computed with a fully second-order discontinuous Galerkin (DG) method applied to the original P_7 system. The DG scheme is taken from [26] and is known to be asymptotic preserving. In particular, for fixed σ, the DG scheme becomes a continuous, finite-element scheme for the diffusion equation in the limit $\varepsilon \to 0$.

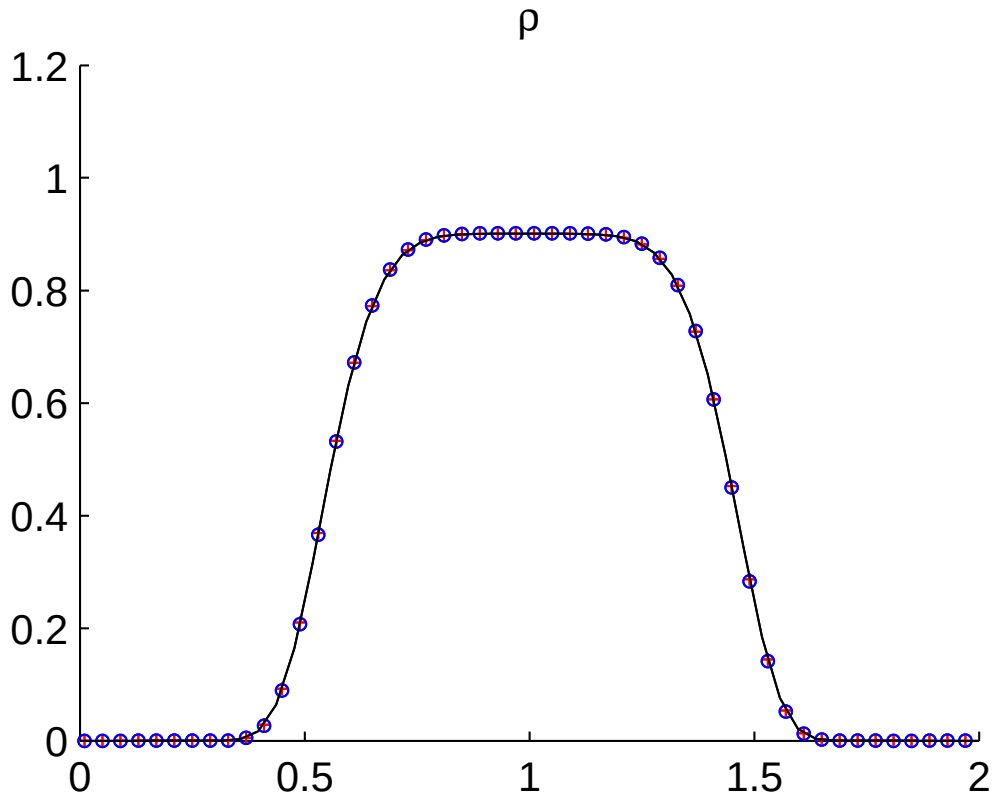

Figure 5: Profile of ρ for the vanishing cross-section (83) at time $t = 0.1$, with $\varepsilon = 10^{-3}$. Circles: RP_7 using wave splitting scheme (78) with $h = 0.02$ and $\Delta t = 2.0 \times 10^{-6}$; solid line: RP_7 using wave splitting scheme (78) with $h = 0.002$ and $\Delta t = 2.0 \times 10^{-7}$; crosses: P_7 using DG scheme from [26] with $h = 0.02$ and $\Delta t = 6.0 \times 10^{-6}$.

5.2.2 Discontinuous Cross-section

In our final experiment, we consider the discontinuous cross-section

$$\sigma(x) = \begin{cases} 0.02, & x \in [0.35, 0.65] \cup [1.35 \cup 1.65]\,, \\ 1.0, & x \in [0, 0.35) \cup (0.65, 1.35) \cup (1.65, 2]\,, \end{cases} \tag{85}$$

and compute solutions to the RP_7 system in (i) a streaming regime ($\varepsilon = 2.0$), (ii) a transition regime ($\varepsilon = 4.0 \times 10^{-2}$), and (iii) a diffusive regime ($\varepsilon = 10^{-5}$). Results of these calculations for the density ρ and the momentum m are shown in Figure (6), where they are again compared to DG results.[2] In the streaming case (Figures 6a-b)), we use the wave-splitting algorithm (80) with flux corrections. The scheme is slightly more dissipative than the DG solver which uses the limiter in (65) with $\theta = 2$. Unfortunately, our implementation of the algorithm is unstable with such a limiter.

In the transition regime (Figures 6c-d)), we see that the first two moments of each scheme give very similar results. There are two minor differences: (i) the DG scheme clips the density profile at $x = 1.0$ and (ii) the small discontinuities in the RP_7 solution for m at $x = 0.65$ and $x = 1.35$ are not present in the DG solution.

In the diffusive regime (Figures 6c-d)), we use the simple wave-splitting algorithm (78) because (80) is unstable. The profile for ρ in the RP_7 solution and the DG solution to P_7 agree quite closely, again with only minor differences at $x = 1.0$. However, the DG solution does a much better job capturing the smooth behavior of m. By breaking up the term $\gamma B \partial_x(\mathbf{u}^k)$ in (71), we have altered the numerical balance for m and for the other higher order moments, and the effect of our treatment becomes more pronounced as ε becomes smaller. In this case, the main benefit of our implementation is the speedup enabled by a fully implicit discretization (since ε is under-resolved). Whereas the DG scheme is explicit, with time step $\Delta t = 6.0 \times 10^{-8}$, our time step is $\Delta t = 2.0 \times 10^{-3}$.

6 Discussion and Conclusion

Using an operator splitting technique, we have derived a system of regularized equations which formally approximate the P_N equations in a slab geometry up to a first order temporal correction. The new system is similar to the original system in the streaming limit; it captures the proper diffusion limit; and it is much less stiff than the original P_N system. Indeed, for under-resolved regimes, there is no hyperbolic time step restriction required to maintain linear stability.

For spatially varying cross-sections, the regularized system is hyperbolic, but contains non-conservative terms. Conventional upwind schemes are not appropriate for such a system, so we have employed a wave-splitting technique developed in [3]. Our results are generally positive; however, when adding higher order corrections to the scheme, there are some stability issues that must be resolved.

There are several important issues about the temporal regularization that should be addressed. Our plans for future work include the following:

[2] All results are cell averages. For the DG scheme, the linear reconstruction of the momentum variable in diffusion regimes often displays a sawtooth behavior.

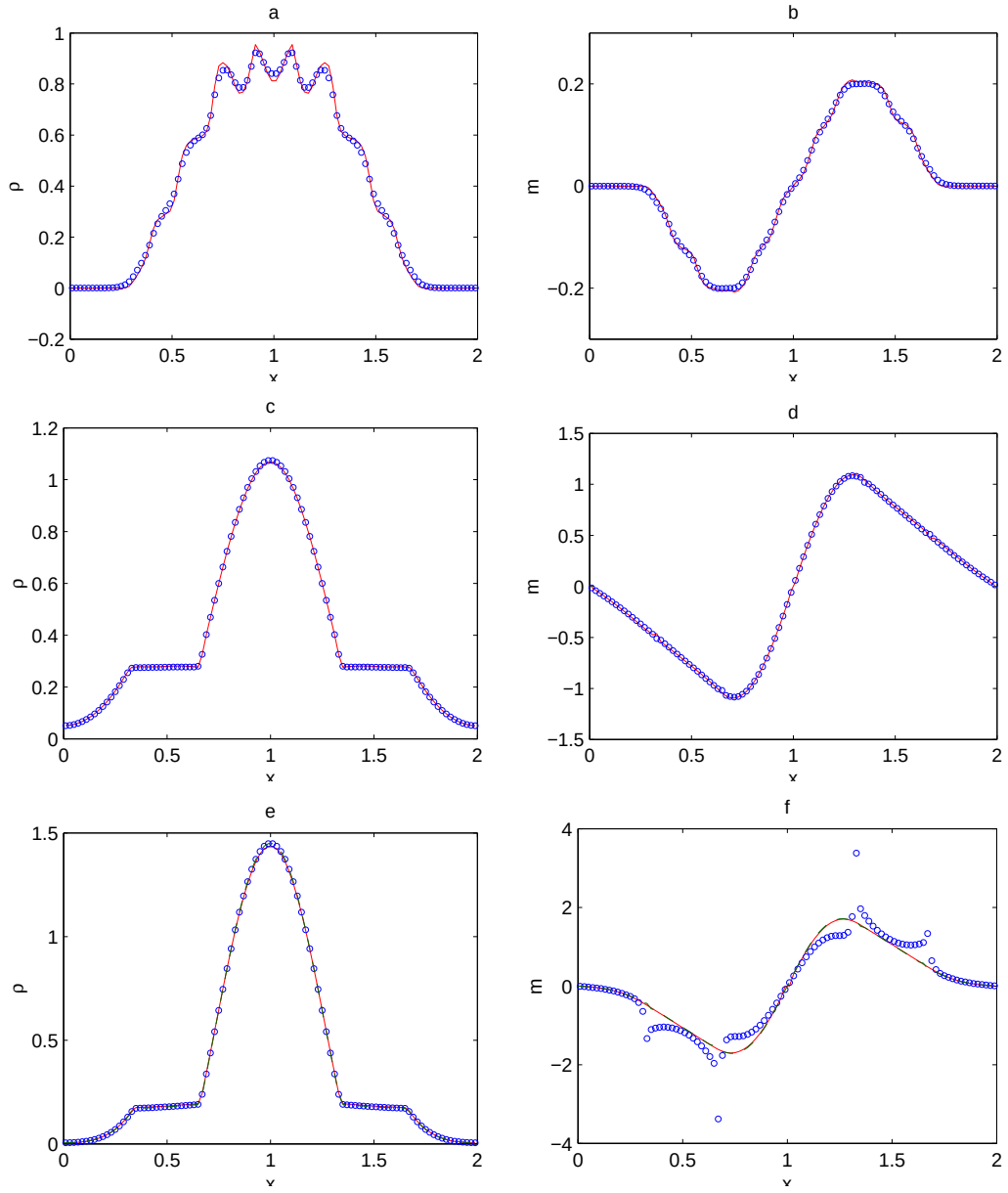

Figure 6: Comparison of RP_7 using wave-splitting scheme (circles) and P_7 using DG scheme (solid line) for the cross-section given in (85). Left plots are ρ and right plots are m. From top to bottom: $\varepsilon = 2.0$, $t = 1.0$; $\varepsilon = 4.0 \times 10^{-2}$, $t = 0.1$; $\varepsilon = 10^{-5}$, $t = 0.05$. In plots (a)-(d) RP_7 solution is computed with wave-splitting scheme with flux corrections (80). In plots (e)-(f), RP_7 solution is computed using the simpler scheme (78). For comparison, the bottom two plots also contain the diffusion limit (dash-dot line), but it is not as visible because of overlap. All computations use mesh spacing $h = 0.02$. For the DG scheme, $\Delta t = 6.0 \times 10^{-8}$. For the RP_7 and diffusion calculations, $\Delta t = 2.0 \times 10^{-3}$.

- **Extension to multiple dimensions, non-linear systems, and systems with more complicated physics.** Of particular interest is thermal radiative transfer, where the cross-section depends on a material temperature that is coupled to the P_N system via a relaxation term. The extension to nonlinear systems is a challenge because, unlike the linear case, function composition does not result in simple matrix multiplication.

- **Improved accuracy.** We would like to improve on the temporal accuracy of our regularization. However, the building blocks of any new method should be systems of hyperbolic-parabolic type in order to avoid high-order (greater than two) spatial derivatives. In developing these methods, one must also consider the "asymptotic target". To leading order, a method must always recover the diffusion equation in the diffusion limit. However, it may be the Chapman-Enskog expansion does not generate the proper target at higher orders of ε.

- **Limiter effects.** We are currently investigating the effects of different limiters and reconstructions for a wide range of ε values, but particularly in diffusive regimes, where ε is small. Our initial experiments have found that limiters affect higher order moments in these regimes. The issue here is that higher order moments becomes spatial gradients of lower order moments in the diffusion limit. Thus slope limiters must be implemented with care. In very diffusive regimes, these moments contribute little to the expansion of F in (15); in such cases, the numerical artifacts introduced by different reconstructions may not matter. However, in transition regimes that are only slightly diffusive, these artifacts may be problematic.

- **Methods for spatially varying cross-sections.** Although our regularization shows promising results, more work is required to develop a robust scheme for the RP_N system with non-constant cross-sections. Any such scheme should maintain conservation of ρ *and* the leading order balances for higher order moments. It should also be able to handle discontinuities in the cross-section which model material interfaces. Current work in this direction is focused on applying the theory of non-conservative products [6, 30].

- **Analytical properties of regularized equations.** The derivation of the RP_N equations in this paper has been purely formal. An important step forward is to establish rigorous results relating the regularized equations to the original P_N system. Part of this analysis will certainly require a deeper understanding of the nonconservative product $\gamma B \partial_x(\mathbf{u}^k)$ from (75)

7 Appendix

Proof of Proposition 3. For simplicity and without loss of generality, we apply the first-order wave-splitting algorithm to (16) without explicitly discretizing in time. Thus the scheme has the form

$$h d_t \mathbf{u}_i + \left(R_\varepsilon^- L_\varepsilon^- \mathbf{\Delta}_{i+1/2} + R_\varepsilon^+ L_\varepsilon^+ \mathbf{\Delta}_{i-1/2} \right) = 0 \,, \tag{86}$$

where

$$\mathbf{\Delta}_{i+1/2} := \left(A + \frac{1}{\varepsilon^2}B\right)(\mathbf{u}_{i+1} - \mathbf{u}_i) - \frac{h\sigma_{i+1/2}}{\varepsilon^2}Q\mathbf{u}_{i+1/2}\,, \tag{87}$$

$\sigma_{i+1/2}$ and $\mathbf{u}_{i+1/2}$ are averages of adjacent cell values, and the matrices $R_\varepsilon^\pm$ and $L_\varepsilon^\pm$ contain right and left eigenvectors corresponding to the positive and negative eigenvalues of $A+\varepsilon^{-2}B$. The first two components of $\mathbf{\Delta}_{i+1/2}$ are

$$[\mathbf{\Delta}_{i+1/2}]_0 = m_{i+1} - m_i\,, \tag{88a}$$

$$[\mathbf{\Delta}_{i+1/2}]_1 = \frac{2}{3}(w_{i+1} - w_i) + \frac{1}{3}\frac{\rho_{i+1} - \rho_i}{\varepsilon^2} + \frac{h\sigma_{i+1/2}}{\varepsilon^2}m_{i+1/2}\,. \tag{88b}$$

For clarity, we use square brackets to separate subscripted indices that denote vector and matrix components from those used to denote mesh cells. Recall from (10) that ρ, m, and w are the first three components of $\mathbf{u}$.

It is not easy to infer the asymptotic behavior of $\mathbf{\Delta}_{i+1/2}$ from (86) because the components of R_ε and L_ε depend on ε. To make the asymptotics more transparent, we express these matrices in terms of the corresponding matrices R and L associated with the matrix $A + B$. The components of R and L are independent of ε; according to Proposition 1,

$$R_\varepsilon^\pm = S_\varepsilon^{-1}R^\pm \qquad \text{and} \qquad L_\varepsilon^\pm = S_\varepsilon L^\pm\,, \tag{89}$$

where $[S_\varepsilon]_{nr} = \varepsilon^n\delta_{nr}$ and $[S_\varepsilon^{-1}]_{nr} = \varepsilon^{-n}\delta_{nr}$ are diagonal matrices.

By applying L_ε^- and L_ε^+ to (86) at cells i and $i+1$, respectively, one can express $\mathbf{\Delta}_{i+1/2}$ as

$$\mathbf{\Delta}_{i+1/2} = -hS_\varepsilon^{-1}R\begin{pmatrix} L^-S_\varepsilon d_t\mathbf{u}_i \\ L^+S_\varepsilon d_t\mathbf{u}_{i+1} \end{pmatrix}. \tag{90}$$

Thus, because of S_ε^{-1}, the asymptotics of each component are

$$[\mathbf{\Delta}_{i+1/2}]_n = hO(\varepsilon^{-n})\,, \quad 0 \le n \le N\,. \tag{91}$$

From (88b) and (91), it follows immediately that

$$m_{i+1/2} = -\frac{1}{3\sigma_{i+1/2}}\frac{\rho_{i+1} - \rho_i}{h} + O(\varepsilon)\,. \tag{92}$$

This is a discrete version of the leading order balance in (22b).

To recover the limiting equation for $\rho \equiv [\mathbf{u}]_0$, we rewrite (86) in the following form:

$$hd_t\mathbf{u}_i + \frac{\mathbf{\Delta}_{i+1/2} + \mathbf{\Delta}_{i-1/2}}{2} = S_\varepsilon^{-1}(R^+L^+ - R^-L^-)S_\varepsilon\frac{[\mathbf{\Delta}_{i+1/2} - \mathbf{\Delta}_{i-1/2}]}{2}\,. \tag{93}$$

When the source term in (87) is zero, equation (93) is just a standard first-order, upwind scheme and the term on the right-hand side is the dissipation term. Taking the first compo-

nent of (93) and using (88a), we have

$$d_t\rho_i + \frac{m_{i+1} - m_{i-1}}{2h} = \sum_{n=0}^{N} [S_\varepsilon^{-1}(R^+L^+ - R^-L^-)S_\varepsilon]_{0n} \frac{[\mathbf{\Delta}_{i+1/2} - \mathbf{\Delta}_{i-1/2}]_n}{2h} \tag{94a}$$

$$= \sum_{n=0}^{N} [(R^+L^+ - R^-L^-)S_\varepsilon]_{0n} \frac{[\mathbf{\Delta}_{i+1/2} - \mathbf{\Delta}_{i-1/2}]_n}{2h} \tag{94b}$$

$$= \sum_{n=0}^{N} \varepsilon^n [R^+L^+ - R^-L^-]_{0n} \frac{[\mathbf{\Delta}_{i+1/2} - \mathbf{\Delta}_{i-1/2}]_n}{2h} \tag{94c}$$

$$= O(h)\,. \tag{94d}$$

Note that the only contribution of S_ε^{-1} in the dissipation term in (94a) is $[S_\varepsilon^{-1}]_{00} = 1$ and that (94d) is computed from (94c) using (91). Finally, by setting $m_{i+1/2} = (m_i + m_{i+1})/2$ in (92) and then substituting the result into (94), we recover a consistent discretization of the diffusion equation (21) in the limit that $\varepsilon \to 0$.

■

Acknowledgements *The authors would like to thank Ryan McClarren, who graciously provided the discontinuous Galerkin results used in Figures 5 and 6. This work was supported by the U.S. Department of Energy at Los Alamos National Laboratory under contracts DE-AC52-06NA25396 and the DOE Office of Science Advanced Computing Research (ASCR) Program.*

References

[1] G. B. Arfken and H. J. Weber, *Mathematical Methods for Physicists*, Academic Press, San Diego, 4th ed., 1995.

[2] E. Audusse, F. Bouchut, M.-O. Bristeau, R. Klein, and B. Perthame, *A fast and stable well-balanced scheme with hydrostatic reconstruction for shallow water flows.*, SIAM J. Sci. Comp., 25 (2004), pp. 2050–2065.

[3] D. S. Bale, R. J. Leveque, S. Mitran, and J. . Rossmanith, *A wave propogation method for conservation laws and balance laws with spatially varying flux functions*, SIAM J. Sci. Comp., 24 (2003), pp. 955–978.

[4] F. Bouchut, G. Ounaissa, and B. Perthame, *Upwinding of the source term at interfaces for Euler equations with high friction*, Computers and Mathematics with Applications, 53 (2007), pp. 361–375.

[5] C. Buet and S. Cordier, *Asymptotic preserving scheme and numerical methods for radiative hydrodynamic models*, C. R. Acad. Sci Paris, Ser. I, 338 (2004), pp. 951–956.

[6] G. DalMaso, P. G. LeFloch, and F. Murat, *Definition and weak stability of nonconservative products*, Journal de Mathematiques Pures et Appliquees, 74 (1995), pp. 483–548.

[7] B. Davison, *Neutron Transport Theory*, Oxford University Press, London, 1973.

[8] F. Filbet and B. P. Ph. Lauren¸ot, *Derivation of hyperbolic models for chemosensitive movement*, J. Math. Biol., 50 (2005), pp. 189–2007.

[9] F. Filbet and C.-W. Shu, *Approximation of hyperbolic models for chemosensitive movement*, SIAM J. Sci. Comp., 27 (2005), pp. 850–872.

[10] S. Goldstein, *On diffusion by discontinuous movements, and on the telegraph equation*, Quart. J. Mech. Appl. Math., 4 (1951), pp. 129–156.

[11] L. Gosse and G. Toscani, *An asymptotic-preserving, well-balanced scheme for the hyperbolic heat equations*, C. R. Acad. Sci. Paris, Ser. I, 334 (2002), pp. 337–342.

[12] ——, *Asymptotic-preserving and well-balanced schemes for radiative transfer and the Rosseland approximation*, Numerische Mathematik, 98 (2004), pp. 223–250.

[13] C. D. Hauck, *Entropy-Based Moment Closures in Semiconductor Models*, PhD thesis, University of Maryland, College Park, 2006.

[14] S. Jin, *Efficient asymptotic preserving (AP) schemes for some multiscale kinetic equations*, SIAM J. Sci. Comp., 21 (1999), pp. 441–454.

[15] S. Jin, L. Pareschi, and G. Toscani, *Diffusive relaxation schemes for multiscale discrete-velocity kinetic equations*, SIAM J. Numer. Anal., 35 (1998), pp. 2405–2439.

[16] ——, *Uniformly accurate diffusive relaxation schemes for multiscale transport equations*, SIAM J. Numerical Analysis, 98 (2000), pp. 913–936.

[17] T. G. Kurtz, *Convergence of sequences of semigroups of nonlinear operators with an application to gas kinetics*, Trans. Amer. Math. Soc., 186 (1973), pp. 259–272.

[18] R. J. Leveque, *Finite Volume Methods for Hyperbolic Problems*, Cambridge Texts in Applied Mathematics, Cambridge University Press, New York, 2002.

[19] C. D. Levermore, *Relating eddington factors to flux limiters*, J. Quant. Spectrosc. Radiat. Transfer, 31 (1984), pp. 149–160.

[20] ——, *private communication*, 2008.

[21] E. E. Lewis and J. W. F. Miller, *Computational Methods in Neutron Transport*, John Wiley and Sons, New York, 1984.

[22] P.-L. Lions and G. Toscani, *Diffusive limit for finte velocity Boltzmann kinetic models*, Rev. Mat Iberoamericana, 13 (1997), pp. 473–513.

[23] R. B. Lowrie and J. E. Morel, *Methods for hyperbolic systems with stiff relaxation*, Int. J. Numer. Meth. Fluids, 40 (2002), pp. 413–423.

[24] P. Marcati and B. Rubino, *Parabolic relaxation limit for hyperbolic systems of conservation laws*, Proceedings of the VIII conference on Waves and Stability, (1996), pp. 393–406.

[25] ——, *Hyperbolic to parabolic relaxation theory for quasilinear first order systems*, J. Differential Equations, 162 (2000), pp. 359–399.

[26] R. G. McClarren, T. M. Evans, R. B. Lowrie, and J. D. Densmore, *Semi-implicit time integration for P_N thermal radiative transfer*, to appear in J. Comp. Phys., (2008).

[27] H. P. McKean, *The central limit theorem for Carlemann's equation*, Israel J. Math, 21 (1975), pp. 54–92.

[28] G. N. Minerbo, *Maximum entropy Eddington factors*, J. Quant. Spectrosc. Radiat. Transfer, 20 (1978), pp. 541–545.

[29] G. Naldi and L. Pareschi, *Numerical schemes for hyperbolic systems of conservation laws with stiff diffusive relaxation*, SIAM J. Numer. Anal., 37 (2000), pp. 1246–1270.

[30] C. Pares, *Numerical methods for nonconservative hyperbolic systems: a theoretical framework*, SIAM Journal on Numerical Analysis, 44 (2006), pp. 300–321.

[31] G. C. Pomraning, *Radiation Hydrodynamics*, Pergamon Press, New York, 1973.

[32] P. L. Roe, *Characterstic-based schemes for the Euler equations*, Ann. Rev. Fluid Mech., 18 (1986), pp. 337–365.

[33] ——, *Upwind Difference Schemes for Hyperbolic Conservation Laws with Source Terms*, vol. 1270 of Lecture Notes in Mathematics, Springer-Verlag, 1986, pp. 41–51.

[34] G. I. Taylor, *Diffusion by continuous movements*, Proc. London Math. Soc., 20 (1921), pp. 196–212.